Coordinated Cluster, ground-based instrumentation and low-altitude satellite observations of transient poleward-moving events in the ionosphere and in the tail lobe

Article

Published Version

Annales
Geophysicae

Coordinated Cluster, ground-based instrumentation and low-altitude satellite observations of transient poleward-moving events in the ionosphere and in the tail lobe

M. Lockwood[1, 2], **H. Opgenoorth**[3], **A. P. van Eyken**[4], **A. Fazakerley**[5], **J.-M. Bosqued**[6], **W. Denig**[7], **J. A. Wild**[8], **C. Cully**[9, 3], **R. Greenwald**[10], **G. Lu**[11], **O. Amm**[12], **H. Frey**[21], **A. Strømme**[13], **P. Prikryl**[14], **M. A. Hapgood**[1], **M. N. Wild**[1], **R. Stamper**[1], **M. Taylor**[5], **I. McCrea**[1], **K. Kauristie**[12], **T. Pulkkinen**[12], **F. Pitout**[3], **A. Balogh**[15], **M. Dunlop**[15], **H. Rème**[6], **R. Behlke**[3], **T. Hansen**[13], **G. Provan**[8], **P. Eglitis**[3], **S. K. Morley**[2], **D. Alcaydé**[6], **P.-L. Blelly**[6], **J. Moen**[16, 17], **E. Donovan**[9], **M. Engebretson**[18], **M. Lester**[8], **J. Watermann**[19], **and M. F. Marcucci**[20]

[1]Solar Terrestrial Physics Division, Space Science and Technology Department, Rutherford Appleton Laboratory, Chilton, Didcot, Oxfordshire, UK
[2]Department of Physics and Astronomy, Southampton University, Southampton, UK
[3]IRF, Swedish Institute of Space Physics, Uppsala Division, Sweden
[4]EISCAT Scientific Association, Longyearbyen, Svalbard, Norway
[5]Mullard Space Science Laboratory, Holmbury St. Mary, Surrey, UK
[6]CESR, Centre d'Etude Spatiale des Rayonnements, Toulouse, France
[7]Space Vehicles Directorate, Air Force Research Laboratory, Hanscom AFB, Massachusetts, USA
[8]Department of Physics and Astronomy, Leicester University, Leicester, UK
[9]University of Calgary, Calgary, Canada
[10]Remote Sensing Group, Applied Physics Laboratory, John Hopkins University, Laurel, MD, USA
[11]High Altitude Observatory, National Center for Atmospheric Research, Boulder, Colorado, USA
[12]Finnish Meteorological Institute, Helsinki, Finland
[13]University of Tromsø, Tromsø, Norway
[14]Communications Research Centre, Ottawa, Ontario, Canada
[15]Blackett Laboratory, Imperial College, London, UK
[16]Department of Physics, University of Oslo, Blindern, Oslo, Norway
[17]Also at Arctic Geophysics, University Courses on Svalbard, Longyearbyen, Norway
[18]Department of Physics, Augsburg College, Minneapolis, MN, USA
[19]Danish Meteorological Institute, Copenhagen, Denmark
[20]Istituto di Fisica dello Spazio Interplanetario - CNR, Rome, Italy
[21]University of California, Berkeley, California, USA

Abstract. During the interval between 8:00–9:30 on 14 January 2001, the four Cluster spacecraft were moving from the central magnetospheric lobe, through the dusk sector mantle, on their way towards intersecting the magnetopause near 15:00 MLT and 15:00 UT. Throughout this interval, the EISCAT Svalbard Radar (ESR) at Longyearbyen observed a series of poleward-moving transient events of enhanced F-region plasma concentration ("polar cap patches"), with a repetition period of the order of 10 min. Allowing for the estimated solar wind propagation delay of 75 ($\pm$5) min, the interplanetary magnetic field (IMF) had a southward component during most of the interval. The magnetic footprint of the Cluster spacecraft, mapped to the ionosphere using the Tsyganenko T96 model (with input conditions prevailing during this event), was to the east of the ESR beams.

Around 09:05 UT, the DMSP-F12 satellite flew over the ESR and showed a sawtooth cusp ion dispersion signature that also extended into the electrons on the equatorward edge of the cusp, revealing a pulsed magnetopause reconnection. The consequent enhanced ionospheric flow events were imaged by the SuperDARN HF backscatter radars. The average convection patterns (derived using the AMIE technique on data from the magnetometers, the EISCAT and SuperDARN radars, and the DMSP satellites) show that the associated poleward-moving events also convected over the predicted footprint of the Cluster spacecraft. Cluster observed enhancements in the fluxes of both electrons and ions. These events were found to be essentially identical at all four spacecraft, indicating that they had a much larger spatial scale than the satellite separation of the order of 600 km. Some of the events show a correspondence between the lowest energy

Correspondence to: M. Lockwood (M.Lockwood@rl.ac.uk)

magnetosheath electrons detected by the PEACE instrument on Cluster (10–20 eV) and the topside ionospheric enhancements seen by the ESR (at 400–700 km). We suggest that a potential barrier at the magnetopause, which prevents the lowest energy electrons from entering the magnetosphere, is reduced when and where the boundary-normal magnetic field is enhanced and that the observed polar cap patches are produced by the consequent enhanced precipitation of the lowest energy electrons, making them and the low energy electron precipitation fossil remnants of the magnetopause reconnection rate pulses.

Key words. Magnetospheric physics (polar cap phenomena; solar wind – magnetosphere interactions; magnetosphere – ionosphere interactions)

1 Introduction

1.1 Poleward-moving transient events in the cusp/cleft

The cusp/cleft aurora, dominated by 630 nm red line emissions from atomic oxygen, shows a series of poleward-moving events when the interplanetary magnetic field (IMF) points southward (e.g. Sandholt et al., 1992; Fasel, 1995). Using the European Incoherent Scatter (EISCAT) UHF and VHF incoherent scatter radars, these cusp/cleft auroral transients have been shown to be associated with transient flow bursts (Lockwood et al., 1989a, b; 1993a, b; Moen et al., 1995; 1996a) and consequent ion-neutral heating of the ionospheric ion gas (Lockwood et al., 1993a, b; 1995a). These events are quasi-periodic with a distribution of repeat intervals between about 1 and 30 min, giving a mean value of about 7 min, but a mode value of about 3 min (Fasel, 1995). This distribution is very similar to that of "flux transfer events" (FTEs) on the dayside magnetopause (Lockwood and Wild, 1993). However, in both cases, the low-period part of the distribution is likely to be set by instrument sensitivity and the criterion used to define events (as demonstrated by a comparison of the results of Kuo et al. (1995) with those by Lockwood and Wild). The transient auroral events are seen to form within the LLBL (cleft) precipitation, near the equatorward edge of the cusp/cleft aurora (Moen et al., 1996b) and subsequently migrate poleward into the regions of the cusp and then the mantle precipitations, which is consistent with the evolution of newly-opened field lines (Lockwood et al., 1989a, b; Cowley et al., 1991b; Sandholt et al., 1992; Lockwood et al., 1993a, c). The transient auroral events in the northern hemisphere also move westward/eastward when the IMF by component is positive/negative (e.g. Lockwood et al., 1993a; Milan et al., 2000), as predicted for the curvature ("tension") force on the newly-opened field lines. The repetitive pattern of formation and motion of these events shows that the patches of field lines are produced by pulses in the reconnection rate (Lockwood et al., 1995a) and not by steady reconnection in the presence of oscillations in the Y component of the magnetic field in interplanetary space

(Stauning, 1994; Stauning et al., 1994, 1995) or in the magnetosheath (Newell and Sibeck, 1993). This pattern of event motion is also consistent with the asymmetric MLT distributions of their occurrence for $B_Y > 0$ and $B_Y < 0$ (Karlson et al., 1996), as discussed by Cowley et al. (1991a).

Pinnock et al. (1993) used HF coherent scatter radars to image these transient flow channels in the cusp/cleft region and Milan et al. (1999) have shown that they are indeed associated with the poleward-moving 630 nm optical transients. In addition, Milan et al. (2000) have shown that the flow channels are also associated with poleward-moving forms seen in global images of the UV aurora. These UV aurora, such as the 557.7 nm (atomic oxygen green line) aurora studied by Lockwood et al. (1993a), are coincident with the sheet of upward field-aligned current of the opposite directed pair that is required to transfer the motion of the newly-opened flux into the ionosphere. Lockwood et al. (2001b) have predicted that these arcs will form at the shear in the longitudinal flow speeds at the boundaries between events. The east-west direction of the flow in the channels seen by HF radars is controlled by the prevailing IMF B_Y (Provan et al., 1998) and their motion, as for the optical transients, is consistent with their occurrence as a function of local time (Provan and Yeoman, 1999; Provan et al., 1999). McWilliams et al. (2000) have shown that the distribution of repeat periods of these enhanced flow events is very similar to the corresponding distributions for 630 nm cusp/cleft auroral transients, as reported by Fasel et al., and for magnetopause FTE events, as reported by Lockwood and Wild. From the ground-based optical observations, global UV images and radar observations, events are found to be typically 100–300 km in latitudinal width and to vary in longitudinal extent up to about 2000 km (Lockwood et al., 1990; 1993a; Pinnock et al., 1995; Milan et al., 2000). Such dimensions and the repetition rates mean that these events are major, and sometimes the dominant drivers of convection (Lockwood et al., 1993a; 1995b; Milan et al., 2000).

1.2 Cusp ion steps

Another predicted signature of pulsed reconnection are discontinuities in the dispersion of injected solar wind ions in the cusp region, called "cusp ion steps" (Cowley et al., 1991b; Lockwood and Smith, 1992, 1994; Escoubet et al., 1992; Lockwood and Davis, 1996). These were first reported in low-altitude satellite data by Newell and Meng (1991). An important part of the prediction of these events was the model of ionospheric flow excitation by Cowley and Lockwood (1992) which predicts that patches of newly-opened flux would be appended directly adjacent to each other. Periods of low or zero reconnection rate between pulses give discontinuous steps in the ion dispersion characteristics at the boundaries between these patches: this is due to the discontinuous change in time elapsed since the field line was reconnected. Modelling of the effects of pulsed magnetopause reconnection has been shown to reproduce the observed simultaneous steps in both downward

moving and upward moving ions in the cusp at middle altitudes, unambiguously demonstrating that these events are caused by pulsed reconnection and not by pulsed plasma transfer across the magnetopause (Lockwood et al., 1998). Cusp ion steps have been seen in association with poleward-moving patches of elevated electron temperature (detected by incoherent scatter radar) by Lockwood et al. (1993b), with poleward-moving cusp/cleft auroral transients by Farrugia et al. (1998) and with poleward-moving flow channel events by Yeoman et al. (1997). Pinnock et al. (1995) found some poleward-moving flow channels (detected by HF radar) were in association with a seemingly different "sawtooth" signature in the cusp ions. However, modelling by Lockwood and Davis (1996) showed that this sawtooth signature was, in fact, the same phenomenon as the cusp ion steps seen by Lockwood et al. (1993b), with the differences arising purely from the longitudinal, as opposed to the more meridional nature of the satellite pass. Recently, Morley and Lockwood (2001) have pointed out that for a general satellite orbit orientation, the form of the dispersion also depends on the amplitude of the reconnection rate pulses: sawtooth signatures will become stepped signatures as the amplitude increases.

1.3 Polar cap patches

The enhanced 630 nm emission in poleward-moving cusp/cleft transients is caused by the hot tail of a heated thermal electron population (Wickwar and Kofman, 1984; Lockwood et al., 1993a). The magnetosheath electron precipitation is responsible for that heating, but not for the direct excitation of the emission. Emission intensity is also enhanced by higher ionospheric plasma concentration, and this too can result in more particles in the hot tail of the distribution with sufficient energy to cause excitation of the 630 nm emission. Patches of enhanced plasma concentration convecting anti-sunward are a common feature of the polar cap during southward IMF (Weber et al., 1984; Sojka et al., 1993, 1994, McEwen and Harris, 1996). These are seen convecting through the cusp/cleft region and into the polar cap (Foster and Doupnik, 1984; Foster, 1989; Lockwood and Carlson, 1992; Valladares et al., 1994; Prikryl et al., 1999a, b) and thus, it is likely that they are the fossil remnants of the poleward-moving cusp/cleft transient events.

1.4 The minima separating transient events

One major unresolved question about both poleward-moving 630 nm cusp/cleft transients and polar cap patches is why minima (in luminosity and plasma concentration, respectively) are seen between them. The successful theory of the cusp ion precipitation is based on the concept that each newly-opened field line evolves in a similar manner, such that the ion characteristics depend only on the time elapsed since reconnection. Although pulsed reconnection gives the discontinuities in their energy dispersion within the cusp/cleft region, magnetosheath ions are found in a single contiguous

region of newly-opened field lines and one would expect this to also be true of the injected magnetosheath electron population. Thus, on its own, this model does not explain the minima between events and an additional mechanism must be invoked (Davis and Lockwood, 1996). A variety of candidate mechanisms have been proposed.

Lockwood and Carlson (1992) interpreted the concentration variations, using the model of ionospheric convection excitation by Cowley and Lockwood (1992) (which led to the prediction of cusp ion steps), as the result of changes in the pattern of flow modulating the entry into the polar cap of the EUV-produced sub-auroral plasma. However, Rodger et al. (1994a, c) pointed out that plasma production by soft particle precipitation (Whitteker, 1977; Watermann et al., 1992; Davis and Lockwood, 1996; Millward et al., 1999) and plasma loss by enhanced electric fields and reaction rates (Schunk et al., 1975; Jenkins, 1997; Balmforth et al., 1998, 1999) must also be significant factors in introducing structure into the plasma concentrations on the time scales for flux tubes to enter the polar cap. In time-varying cases, it may be possible for some flux tubes entering the polar cap to have undergone one or both of these processes to a greater degree than others. Lockwood et al. (2000) argued that variation may also be brought about by local time variations in the injected magnetosheath electron population and in the tension force on the newly-opened field lines, provided that the events are sufficiently extensive in longitude. Another possibility, modelled by Davis and Lockwood (1996), is that the electron precipitation spectrum hardens in regions of upward field-aligned currents, such that the underlying E-region is enhanced rather than the F-region. Lockwood et al. (1993a; 2001b) have presented evidence that this does occur in the expected locations since both green line and UV auroral transients on the relevant edge of the patches on newly-opened flux can be identified.

The present paper considers another potential explanation that has not been considered previously. It presents the first observations of ionospheric polar cap patches that can be associated with electron flux variations in the high-altitude mantle region, i.e. near the sunward edge of the tail lobe at a geocentric distance of around 10 R_E (a mean Earth radius, 1 $R_E = 6370$ km). These data strongly imply that some of the patches are produced by modulations in the lowest energy of magnetosheath electrons, caused either by a potential barrier of varying amplitude at the magnetopause or by fluctuations in the electron spectrum present in the magnetosheath before the reconnection occurred. The IMF in the interval studied was predominantly southward (Sect. 2.1). The ionospheric measurements of patches are made by the EISCAT Svalbard radar (ESR), which tracked the patches as they migrated poleward into the polar cap (Sect. 2.3). The lobe measurements were made by the four Cluster-2 spacecraft (Sect. 2.6). Low-altitude satellite data reveal cusp ion steps (Sect. 2.2). Data from the SuperDARN HF coherent radars and magnetometers also reveal fluctuations in the characteristic repeat period of the order of 10 min (Sect. 2.5). Therefore, we discuss all the data (from Cluster, from the ground-
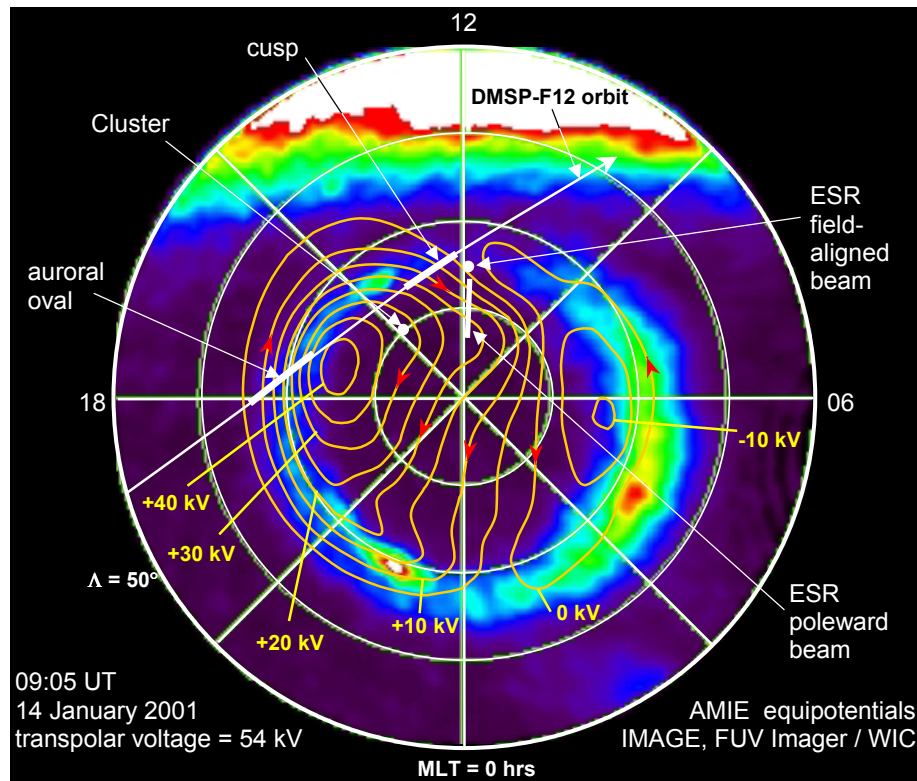
Fig. 1. The locations of the coordinated measurements on 14 January 2001 in an invariant latitude (Λ), with magnetic local time (MLT) frame at 09:05 (the time of the closest approach of the DMSP-F12 satellite to the ESR field-aligned beam). The footprint of the centroid of the Cluster tetrahedron is mapped down to the northern hemisphere ionosphere using the Tsyganenko T96 model with average input parameters for the interval studied here (see text for details). The plot also shows in white the locations of the two beams employed by the EISCAT Svalbard Radar (ESR) on this day. The pass of the DMSP-F12 satellite at 08:54–09:12 UT is shown, with thicker segments denoting where the satellite intersected the dusk auroral oval and the cusp. The orange contours are convection equipotentials, derived by the AMIE technique employing magnetometer, SuperDARN, DMSP and ESR observations. These are superposed on observations of auroral emissions made at this time by the WIC of the FUV imager on the IMAGE satellite.

based instruments and from low-altitude spacecraft) in terms of the effects of pulsed magnetopause reconnection (Sect. 3).

2 Observations

2.1 Overview and interplanetary conditions

On 14 January 2001, the four Cluster spacecraft approached the magnetopause from the tail lobe, following a path close to the 15:00 MLT meridian. Simultaneous measurements were made using a wide array of ground-based instrumentation. An overview of this pass and of the instrumentation deployed is given by Opgenoorth et al. (2001, this issue). Figure 1 is an invariant latitude (Λ) – magnetic local time (MLT) plot of the locations of the various observations at 09:05 on this day. The plot also shows the flow equipotentials and the location of Far Ultraviolet (FUV) auroral emissions at this time (see Sects. 2.5 and 2.6, respectively). The magnetic footprint of the Cluster spacecraft was mapped to the ionosphere using the Tsyganenko T96 model with input conditions observed by ACE at 07:50 UT (IMF $B_X = -3$ nT, $B_Y = +2$ nT,

$B_Z = -3$ nT, solar wind concentration $N_{sw} = 2.0$ cm^{-3} and velocity $V_{sw} = 400$ km s^{-1}, giving a dynamic pressure $P_{sw} = 0.6$ nPa) and with the geomagnetic index of Dst $= 0$. These input conditions are based on a derived propagation delay from ACE to the magnetosphere of 75 min (see below). Also shown in Fig. 1 are the two beams of the ESR (Mc-Crea and Lockwood, 1997), deployed pointing along the geomagnetic field line from Longyearbyen and with a 30° elevation along the magnetic meridian to the north, and the pass of the low-altitude DMSP (Defense Meteorological Satellite Program) F12 satellite, as it moved equatorward through the cusp, with the closest conjunction to Svalbard at 09:05 UT.

Figure 2 presents three views of the Cluster orbit in Geocentric Solar Ecliptic (X_{GSE}, Y_{GSE}, Z_{GSE}) coordinates, along with the mapped field lines of the type that gave the footprint shown in Fig. 1. The top, middle and bottom panels are for the projections onto the (X_{GSE}, Y_{GSE}), (X_{GSE}, Z_{GSE}) and (Y_{GSE}, Z_{GSE}) planes, and the solid and dashed blue lines show the model magnetopause and bow shock locations for $Z_{GSE} = 0$, $Y_{GSE} = 0$, and $X_{GSE} = 0$, respectively, predicted using the magnetopause model by Shue et al. (1997) and the bow shock model by Peredo et al. (1995). The Cluster or-

bit is shown in black and traced field lines are shown from the spacecraft locations at 04:00, 08:00 and 12:00 UT. Field lines mapped to the local (northern) hemisphere are shown in green, and those mapped to the southern hemisphere are in red.

By about 9:00 UT, the Cluster spacecraft were in the mantle region of the northern tail lobe (see Opgenoorth et al., 2001, this issue) and were predicted by the field line model to be close to the L-shell sampled by the furthest range gates of the low elevation ESR beam, but considerably to the east (near 15:00 MLT, whereas the ESR beams are near 12:00 MLT). At this time, the DMSP-F12 satellite intersected the cusp, very close to the ESR field-aligned beam at noon. Subsequently, the ESR beams rotated around toward the 15:00 MLT meridian and the closest conjunction with Cluster was at 12:22 UT, as predicted by this magnetic field model. Cluster particle observations reveal that the four spacecraft passed from the mantle region into the low-latitude boundary layer (LLBL) at about 10:45 and into the dayside boundary plasma sheet (BPS) at around 11:00; these changes appear to be a response to a northward turning of the IMF, causing the dayside polar cap boundary to contract poleward and the magnetopause to expand outward (see below). The exterior particle cusp and the magnetopause intersection observed later in the pass are discussed in the paper by Opgenoorth et al. (2001, this issue) and the transient entries of the satellites into the LLBL from the BPS between 11:00 and 13:00 are studied by Lockwood et al. (2001a, this issue). In the present paper, we concentrate on the data taken between 08:00–09:30, including the close conjunction between the ESR and DMSP-F12 at 09:05. The low-altitude of DMSP-F12 (near 840 km) means that there is very little uncertainty in the time and position of its closest magnetic conjunction to the ESR (Lockwood and Opgenoorth, 1997). However, one must bear in mind the long distances over which field lines have been traced in Fig. 2 (using an averaged empirical model that attempts to close all geomagnetic flux); the Cluster footprint locations are thus highly model dependent and give us only a rough indication of where the spacecraft were in relation to the ground-based instrumentation and the DMSP-F12 pass.

Panels (a), (b) and (c) of Fig. 3 give the three components of the IMF in GSM coordinates, as seen by the Advanced Composition Explorer (ACE) satellite near to the L1 point. Opgenoorth et al. (2001, this issue) report a very high cross-correlation of the clock angle of the magnetosheath field (in the GSE $Z-Y$ plane), as seen by Cluster once it had emerged from the magnetosphere at about 15:00 UT, with the same angle seen by ACE. The conservation of clock angle across the bow shock means that the correlation coefficient is very high and very significant, and the lag of peak correlation (74 min.) is a good estimate of the propagation delay between ACE and the magnetopause at 15:00 UT. In Fig. 3, we estimate the lag in a different manner for 7:00–12:00 by comparing the Z- and Y-components of the IMF, seen by ACE in GSM coordinates, with the X-component (northward) of the perturbation to the geomagnetic field ΔB_X, as seen by 5 ground-based
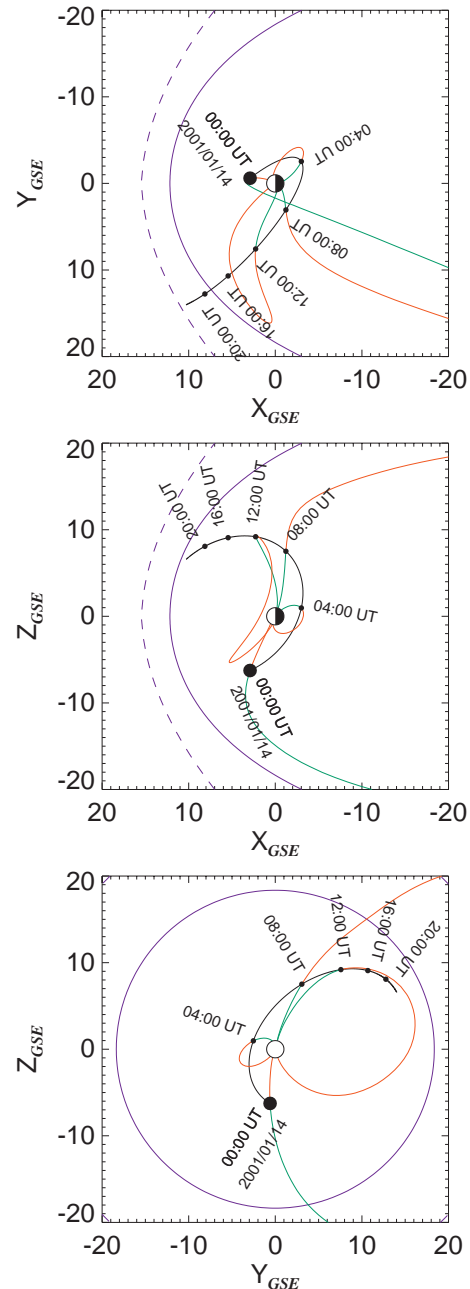

Fig. 2. The Cluster orbit in Geocentric Solar Ecliptic (X_{GSE}, Y_{GSE}, Z_{GSE}) coordinates (in black) along with the mapped field lines that give ionospheric footprints, such as that shown in Fig. 1. **(a)**, **(b)** and **(c)** are projections onto the (X_{GSE}, Y_{GSE}), (X_{GSE}, Z_{GSE}) and (Y_{GSE}, Z_{GSE}) planes and the solid and dashed blue lines show the model magnetopause and bow shock locations for $Z_{\mathrm{GSE}} = 0$, $Y_{\mathrm{GSE}} = 0$, and $X_{\mathrm{GSE}} = 0$, respectively, predicted using the magnetopause model by Shue et al. (1997) and the bow shock model by Peredo et al. (1995). Traced field lines are shown from the spacecraft locations at 04:00, 08:00 and 12:00 UT. Field lines mapped to the local (northern) hemisphere are shown in green, and those mapped to the southern hemisphere are in red.

magnetometers of the IMAGE chain (Syrjäsuo et al., 1998) at Ny Ålesund (NAL, Fig. 3e), Longyearbyen (LYR, Fig. 3f),

Hopen (HOP, Fig. 3g), Bear Island (BJN, Fig. 3h), and Tromsø (TRO, Fig. 3j). A correlation with the IMF B_Y is expected due to the Svalgaard-Mansurov effect, which is due to the magnetic curvature ("tension") force on newly-opened field lines, and also with the IMF B_Z since it controls the production of such newly-opened field lines. The maximum correlation coefficients (with corresponding lags) of B_Y for NAL and LYR are 0.58 (73 min) and 0.55 (72 min), respectively. The corresponding numbers for IMF B_Z, and NAL and LYR are 0.77 (76 min) and 0.71 (75 min), respectively. Note that the use of a 3-hour sliding window shows that the lag of peak correlation varies between about 70 and 80 min. By using the Fischer-Z test for a significant difference in the correlation coefficient, we find the uncertainty in the lag at any one time is typically ±5 min. Figure 3d repeats the IMF B_Z variation, this time on the same time axis as the ionospheric measurements (parts e–k), i.e. shifted by the best-fit propagation lag of 75 min.

Figure 3 marks three periods of special interest: A, B and C. Allowing for the average lag of 75 min, these intervals correspond to 8:00–9:30 UT, 11:19–11:27 UT and 12:00–12:20 UT, respectively, in the ionosphere. We will study period A in detail in this paper; periods B and C are the subject of a subsequent paper by Lockwood et al. (2001a, this issue).

The magnetic perturbations seen on the ground show control by both IMF B_Z and B_Y. In both cases, the lag is slightly longer for NAL, which is poleward of LYR, indicating a poleward motion. Deflections are considerably weaker at Tromsø, placing the open-closed field-line boundary (OCB) somewhere between there and Bear Island, which is consistent with particle observations by DMSP-F12 (see next section).

Figure 3 shows that throughout interval A (08:00–09:30 UT in the ionosphere), the IMF was predominantly southward with a B_Z component in GSM primarily in the range between −2 and −4 nT, with only brief northward excursions. The B_X component is negative throughout, and the B_Y component is negative for the majority of this interval, but with some positive excursions. The solar wind data (not shown) reveal that the solar wind velocity V_{sw} during interval A was roughly constant (varying between 365 and 400 km/s, but close to 368 km/s for the majority of the time). The average number density N_{sw} was initially $6 \cdot 10^6$ m^{-3}, falling to a minimum of about $2 \cdot 10^6$ m^{-3} (at the 08:00 observation time, 09:15 lagged time) before rising again to $5 \cdot 10^6$ m^{-3} by the end of the interval. The fluctuations in the average dynamic pressure, $P_{sw} = <m_i> N_{sw} V_{sw}^2$ (where $<m_i>$ is the mean ion mass) primarily follow those in N_{sw} and thus, also show a variation (50% about the mean of 1.1 nPa in interval A). Subsequently, P_{sw} fell even further, so by intervals B and C, it was only 0.6 nPa on average; for comparison, the mode value of the overall distribution of P_{sw} is close to 3 nPa (Hapgood et al., 1991).

Figure 3j shows the transpolar voltage deduced by fitting an IMF-dependent potential contour model to the line-of-sight velocity data from the SuperDARN radars (Ruohoniemi et al., 1989). The effect of the northward turning of the IMF

is seen just before 11:00 as a decrease in transpolar voltage and an increase in ΔB_X at all stations. In the 2-minute voltage data shown in Fig. 3i, 17 peaks can be defined between 08:00 and 11:00 UT. Each can be associated with a minimum in the ΔB_X at BJN and HOP, and these data series give a repeat interval of the order of 10 min (as seen in the ESR data for the same interval, see Sect. 2.3).

Figure 3 stresses that the responses to the IMF changes with a lag of 75(±5) min were seen at a range of latitudes at the MLT of the ESR and also in the transpolar voltage. It can be seen that around the time of Fig. 1 and the cusp crossing by DMSP-F12 (09:05–09:07 UT, marked by a dot-dashed line in Fig. 3), neither B_Y nor B_Z were stable in their polarity. To within the lag uncertainty of ±5 min, we can define the appropriate average IMF conditions to have been $B_X = -3$ nT, $B_Y = +2$ nT, $B_Z = -3$ nT.

2.2 DMSP-F12 observations

Figure 4 shows energy-time spectrograms (a) for electrons and (b) for ions, as observed by the Defense Meteorological Satellite Program (DMSP)-F12 spacecraft as it passed along the path given in Fig. 1. In both cases, the differential energy flux is plotted as a function of energy (increasing upward) and observation time. Before the satellite entered the polar cap, it passed through an auroral oval showing a series of inverted-V electron arcs at 08:59–09:02 UT. It then entered the polar cap at a magnetic latitude close to 71° and an MLT of 17:00. The purple line in Fig. 4c shows the horizontal convection velocity perpendicular to the satellite track and this changed from sunward to weakly anti-sunward close to the poleward edge of this auroral oval. The satellite was then briefly within the polar cap precipitation region until about 09:03, when it began to observe mantle precipitation and at 09:05, it observed cusp ions and electrons which persisted until 09:07. The cusp was seen between magnetic latitudes of 73.7–75.9°, over the MLT range 13:54–12.12 hrs. Within the cusp, convection flows were anti-sunward, stronger and highly structured. The green line in Fig. 4c shows that in the cusp, vertical flows were structured, pointing upward around 500 m/s, but were downward in the polar cap. The thicker segments of the pass shown in Fig. 1 mark the locations where DMSP-F12 observed the dusk auroral oval and the cusp.

The magnetosheath ions show a structured dispersion. This structure is not as straightforward as the examples presented by Newell and Meng (1991), Lockwood et al. (1993b) and Pinnock et al. (1995); nevertheless, clear upward discontinuities can be seen in the cusp ion lower cutoff energy, E_{ic}. The first major discontinuity is an upward step in E_{ic}, consistent with a stepped cusp. This is followed by a fall and subsequent rise in E_{ic}, which is not fully consistent with either a stepped or a sawtooth cusp ion signature. Thereafter, the cusp takes on the classic sawtooth appearance with a gradual fall in E_{ic} followed by an upward step and then two isolated patches of the higher energy cusp ions, showing features that were all observed by Pinnock et
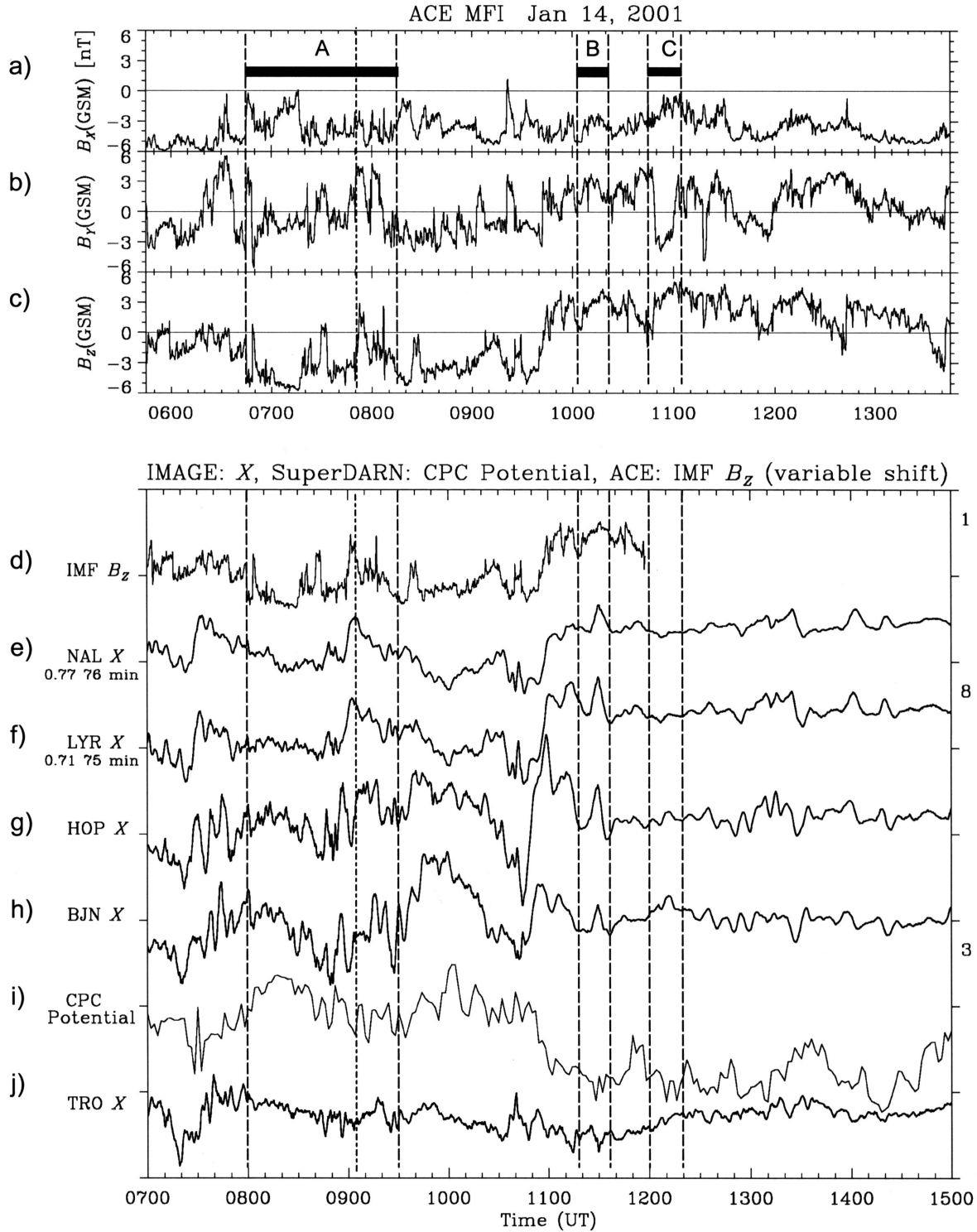
Fig. 3. **(a)** to **(c)** The components B_X, B_Y and B_Z of the interplanetary magnetic field (IMF) in GSM coordinates, as seen by the ACE satellite near to the L1 point. Interval A relates to the present paper, intervals B and C are studied in detail by Lockwood et al. (2001a, this issue). **(d)** The IMF B_Z component shown in 3a, but here lagged by the optimum propagation delay from ACE to the dayside ionosphere of 75 min. Also shown on this time axis are the X components (northward) of the perturbation to the geomagnetic field seen by 5 magnetometers of the IMAGE chain at **(e)** Ny Ålesund (NAL), **(f)** Longyearbyen (LYR), **(g)** Hopen (HOP), **(h)** Bear Island (BJO) and **(j)** Tromsø (TRO). Panel **(i)** shows the transpolar voltage derived from a convection model fit to the SuperDARN data. Allowing for the lag of 75 min., intervals A, B and C correspond to 8:00–9:30 UT, 11:19–11:27 UT and 12:00–12:20 UT, respectively, in the dayside ionosphere.
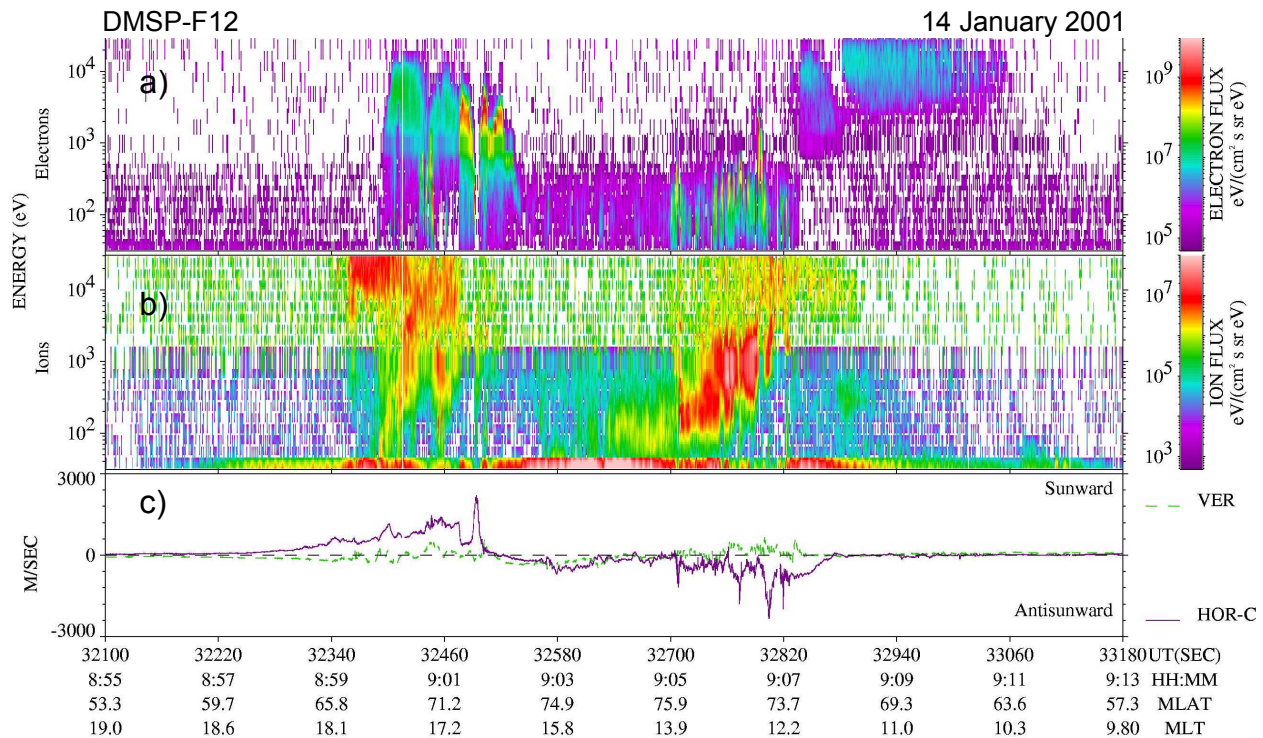
Fig. 4. Energy-time spectrograms for **(a)** electrons and **(b)** ions observed by DMSP-F12 as it passed equatorward along the path given in Fig. 1. In both cases, the differential energy flux is plotted as a function of energy (increasing upward) and observation time, t_s. **(c)** shows the vertical (green) and horizontal (purple) components of the ion velocity (the horizontal component is perpendicular to the satellite track such that positive values have a sunward component and negative values an anti-sunward component).

al. (1995) and modelled by Lockwood and Davis (1996). We would expect a sawtooth signature for such a longitudinal cusp pass in the presence of pulsed reconnection, unless the reconnection pulses have very small amplitude (Morley and Lockwood, 2001). The evolution of the cusp ion signature shown in Fig. 4b reveals reconnection pulses that were initially small, and then subsequently grew in amplitude. The sawtooth dispersion is seen to extend to the high-energy electrons; magnetospheric BPS electrons were seen at energies above 1 keV at almost exactly the same time that the magnetosheath electrons (below 1 keV) disappeared (defining the "electron edge", Gosling et al., 1990; Onsager et al., 1993; Onsager and Lockwood, 1997). However, these BPS electrons subsequently disappeared again in a dispersed manner (higher energies disappearing first) before reappearing, at all energies simultaneously, just after 09:08. Although not uncommon in cusp ions, this is the first time that such a sawtooth signature has been reported to extend into electron data: it is clearly seen in this case due to of the increasing amplitude of the reconnection pulses, with the pulse that provides the electron sawtooth representing the largest of the series. Given that electrons travel very quickly down field lines, we can identify the location of the electron edge as very close to the open-closed boundary (OCB) (see Lockwood, 1997a); the onset of energetic magnetospheric electrons marks the passage of the satellite from open to closed field lines. The

OCB then erodes equatorward in response to a reconnection pulse which is sufficiently large enough in amplitude to cause the OCB to overtake the satellite. This, in turn, causes the electrons to disappear, with the most energetic electrons escaping first through the magnetopause. Subsequently, the equatorward motion of the OCB slowed, allowing the satellite to overtake it again, and causing the BPS electrons to reappear at all energies. These data not only show that reconnection was pulsed, but also show the location of the OCB near 12:00 MLT oscillating in invariant latitude between 71.5° and 73.7° in the interval 09:07– 9:08 UT. This places the ESR field-aligned beam (at invariant latitude 75.1°) on open field lines within (but near the poleward edge) the cusp, as seen by DMSP-F12.

2.3 EISCAT Svalbard radar observations

Figure 5 shows 2-minute post-integrations of the ESR radar observations of plasma concentration in the interval 07:15– 11:45 UT. The top panel is for the low-elevation northward beam and the lower panel is for the field-aligned beam; the plasma concentration is contoured as a function of invariant latitude and observation time in the top panel, and as a function of altitude and observation time in the lower panel. (The contour level scales used are the same as in Fig. 6a). The poleward-pointing beam observed a series of high-density
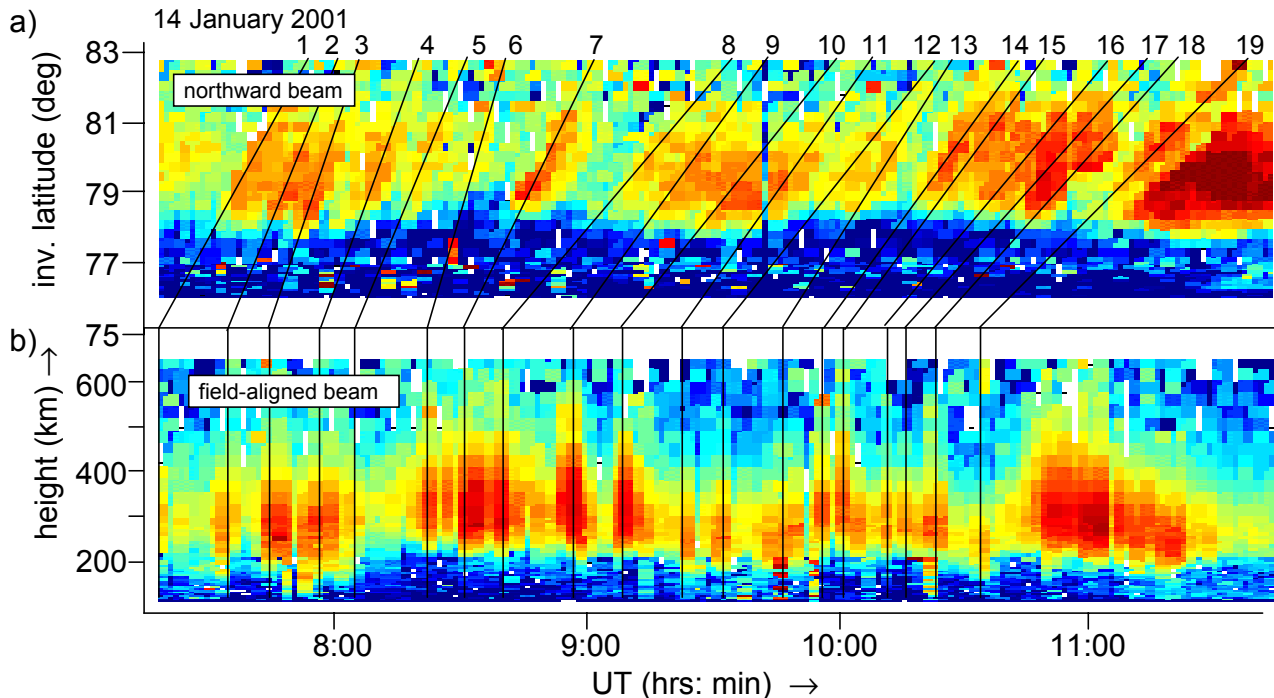
Fig. 5. Two-minute post-integrations of the ESR radar observations of plasma concentration in the interval between 07:15–11:45 UT. **(a)** is for the low-elevation, northward beam and **(b)** is for the field-aligned beam, and the plasma concentration is contoured as a function of invariant latitude and observation time in the top panel and as a function of altitude and observation time in the lower panel. (The contour levels are given by the scale shown for the top panel of Fig. 6). Lines map the centres of poleward-moving events seen in the low-elevation beam back to the invariant latitude of 75.1° of the field-aligned beam.

plasma regions (polar cap "patches") moving along the beam to higher latitudes. These are similar to those seen by lower-latitude radars (Chatanika and the EISCAT UHF and VHF mainland radars), using similar modes of operation with poleward-pointing beams at low elevation, but only when the polar cap is considerably expanded (e.g. Foster and Doupnik, 1984, Lockwood and Carlson, 1992). Since their poleward phase motion was roughly constant in speed, a straight line can be placed through each of these events. These lines have been mapped back to an invariant latitude of 75.1°, representing the location of the field-aligned ESR beam. Fig. 5 shows that the events seen in the field-aligned beam generally match those subsequently seen propagating poleward in the low-elevation beam. The relationship of similar events in the ESR field-aligned beam to phenomena, such as poleward moving flow channels seen by the CUTLASS HF radar and poleward-moving 630 nm auroral transients, has been studied by McCrea et al. (2000) and Lockwood et al. (2000).

This match between the plasma concentration data seen in the two ESR beams persists until the first effects of the northward turning of the IMF, shown in Fig. 3, reaches the magnetosphere at around 10:45. Thereafter, the signatures do not correspond and they do not share a common origin (Blelly et al., 2001, private communication). While patches are passing over both beams, the field-aligned beam gives a detailed picture of the altitude profile of the plasma parameters in each event as it passes over the radar, as presented in Fig. 6. These data have a lower post-integration time of 1 min which is the optimum compromise between the time resolution and the signal-to-noise ratio for the field-aligned beam. The altitude profiles of the events show that most of the plasma concentration (N_e) enhancements were primarily above 150 km (top panel Fig. 6); this altitude corresponds to about 76.5° invariant latitude for the poleward-pointing beam and thus, the events are not generally seen at lower latitudes since the low elevation beam is underneath the N_e events close to the radar. Similarly, the enhancement is small above about 600 km and so altitude effects also indicate that events are not generally detected at invariant latitudes above about 82°. By taking the time series of the data observed in the range gate of the two beams that are at a 300 km altitude, and cross-correlating with a 1-hour running window, gives cross-correlation coefficients between 0.75 and 0.9. (These fall to lower values if longer windows are used due to of the variations in the poleward phase speed of the events).

The lower panels of Fig. 6 show the electron temperature, T_e, the field-aligned ion temperature $[T_i]_{\parallel}$ and the field-aligned ion velocity, $V_{\parallel}$. The electron temperatures, T_e, seen in the field-aligned beam were higher and more structured when the IMF was southward (average values at 300 km, for example, were about 3000 K, compared to about 1500 K after 11:00, when the IMF was predominantly northward (see
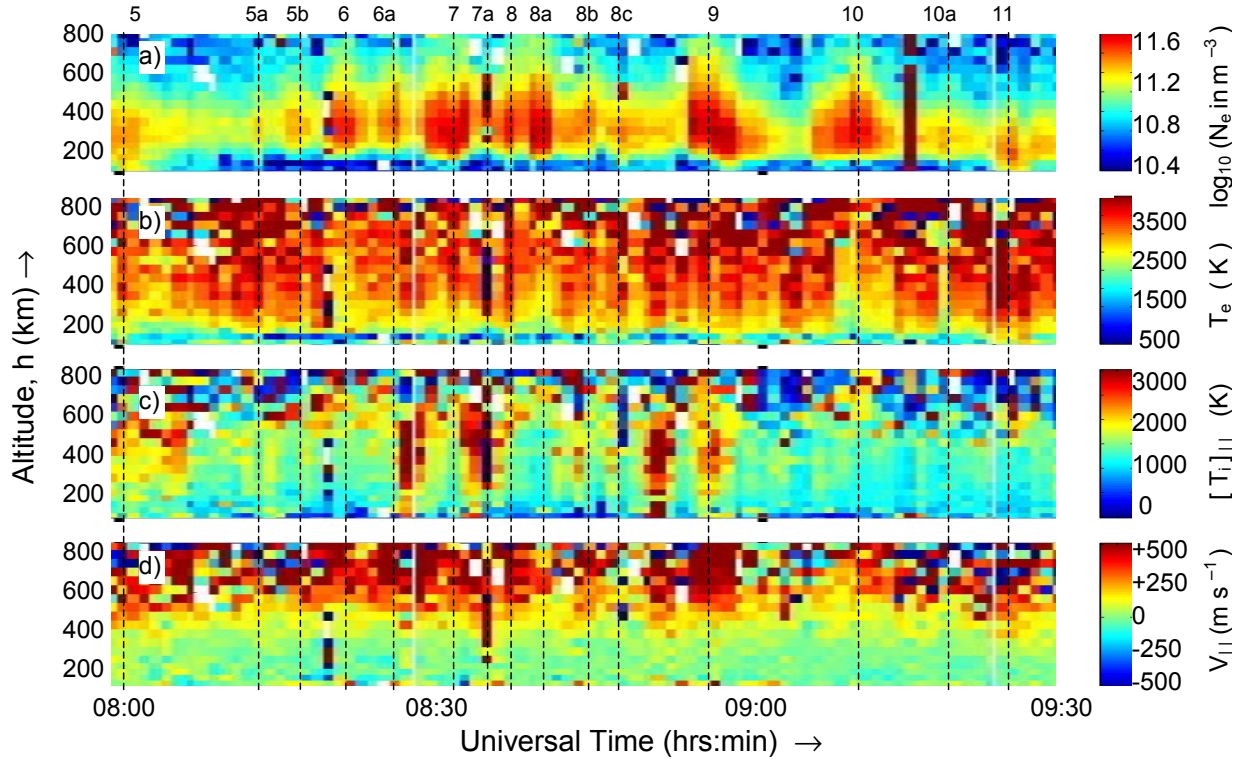
Fig. 6. One-minute post-integrations of the data from the field-aligned ESR beam for 08:00–09:30. Altitude profiles are shown for (from top to bottom): **(a)** the plasma concentration, N_e; **(b)** the electron temperature, T_e; **(c)** the field-aligned ion temperature, $[T_i]_\parallel$ and **(d)** the field-aligned (line-of-sight) ion velocity, $V_\parallel$. The dashed lines mark the centre of events 5, 6, 7, 8, 9, 10, and 11 in this interval, as defined in Fig. 5. These higher-resolution N_e data in the field-aligned direction reveal additional events 5a, 5b, 6a, 7a, 8a, 8b, 8c, and 10a.

Opgenoorth et al. 2001, this issue). The parallel ion temperatures, $[T_i]_\parallel$, showed brief transient enhancements (up to 3000 K, compared with to the background level of 1300 K) and persistent fast, upward flows (with speeds $V_\parallel$ of 300 m/s or more at 500 km) were also observed, but when the IMF was southward.

The ion temperature behaviour is dominated by the largest two terms in the ion thermal balance equation (Lockwood et al., 1993d; McCrea et al., 1993) such that the field-parallel ion temperature is:

$$[T_i]_\parallel = T_n + \frac{\beta_\parallel m_n}{2k} |V - U|^2 , \qquad (1)$$

where T_n is the temperature and m_n is the mean mass of the neutral gas atoms/molecules; $\beta_\parallel$ is the temperature partition coefficient; k is Boltzmann's constant; V and U are the ion and neutral gas velocity vectors, respectively. The coefficient $\beta_\parallel$ has a minimum value of zero (the "relaxation model" of ion-neutral collisions which would be valid for charge exchange with no momentum exchange) and a maximum value of 2/3 (for isotropic scattering). A lower $\beta_\parallel$ corresponds to a higher temperature anisotropy. McCrea et al. (1993) found that $\beta_\parallel$ was about 1/3 near 300 km, but rose to values closer to 2/3 at greater altitudes since the isotropising effects of ion-ion collisions became as important as the anisotropic heating effect of ion-neutral collisions. At the highest altitudes, heat

conduction from the electron to the ion gas may become important since electron temperatures are generally higher. The fact that $\beta_\parallel > 0$ means that differences between V and U result in rises in $[T_i]_\parallel$ that can be detected by the field-aligned ESR beam. Recently, Lockwood et al. (2000) have studied ESR observations of ion heating in and around transient poleward-moving events, as seen by optical instruments and the CUTLASS HF radars. They found that the behaviour depends on the time in the evolution of events at which the radar intersects them. This occurs because the enhanced ion flows V in the events evolve as they change from moving longitudinally under the magnetic curvature force ("tension"), associated with the IMF B_Y component, to poleward motion under the influence of the solar wind flow (Lockwood et al., 1989a, b), whereas the neutral flows U can only show an average response to these changing ion flows. This introduces great variability into the ion temperatures caused by ion frictional heating, even if the interplanetary conditions are stable.

In the interval 07:15–10:50, 19 poleward-moving events were seen in the 2-min resolution data from the field-aligned ESR beam (Fig. 5), all of which can be subsequently identified in the poleward-pointing beam. This gives an average repetition interval of the order of 10 min. Figure 6 shows the 1-min integrated data for the field-aligned beam for the interval A, and an additional 8 events can be seen in these
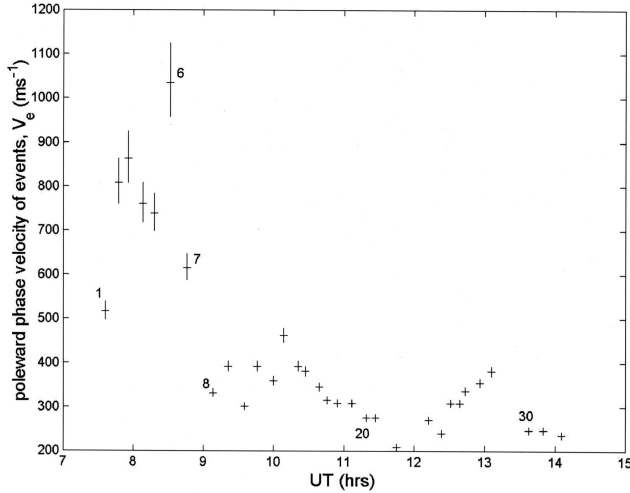
Fig. 7. The phase velocity of the poleward motion of the events, V_e (from the slope of the fitted lines in the top panel of Fig. 5). The events are plotted at the time that they are at invariant latitude of $79°$ and selected events have been numbered for comparison with Fig. 5. Events after 11:00 (21–32) are discussed by Lockwood et al. (2001a, this issue).

higher-resolution data (labelled 5a, 5b, 6a, 7a, 8a, 8b, 8c, and 10a). Of these, event 7a appears to be caused by a bad fit to the data; it is only present in one post-integration period, The altitude profile in N_e is unlike that in any other event and anomalous values are also seen in T_e, $[T_i]_\parallel$ and $V_\parallel$. Neglecting 7a means that we identify a total of 14 events in these data in interval A, giving a mean repeat period of 6.4 min, which is considerably less than the 10 min derived from the 2-min integrated data and from the poleward beam.

Figure 6 reveals that the signatures in the various parameters measured (N_e, T_e, $[T_i]_\parallel$ and $V_\parallel$) have complex relationships and indicate that a number of factors may have contributed to the observed structure in the plasma concentration. Events 6, 8a, 8c, 10 and 10a show decreases in electron temperature T_e coincident with the rises in N_e. Events 8b, 8c and 9 show (generally weak) simultaneous rises in field-parallel ion temperature $[T_i]_\parallel$. However, the major rises in $[T_i]_\parallel$ are between events (e.g. between 6a and 7, 7 and 8, 8c and 9). Event 9 (which shows high N_e, T_e and $[T_i]_\parallel$) reveals a strong burst of upflow velocity, $V_\parallel$, and hence, ion flux $N_e V_\parallel$.

Figure 7 plots the phase velocity of the poleward motion of the events, V_e (from the slope of the fitted lines in the top panel of Fig. 5). The events are plotted at the time that they are at an invariant latitude of $79°$ and selected events have been numbered for comparison with Fig. 5. Events after 11:00 (21–32) are discussed by Lockwood et al. (2001a). It should be noted that three factors enter into the values of V_e: the poleward convection speed, the orientation of the events and the east-west convection speed. Thus, V_e depends on both the B_Y and B_Z components of the IMF, and the orientation of the events will evolve systematically as the radar moves from near noon in MLT into the mid-afternoon sector.

2.4 Magnetometer observations

Figure 8d shows the "upward continuation" of the X-component of the magnetic field $B_X{}'$ (derived as a function of latitude from the IMAGE magnetometer chain). The technique used employs Fourier analysis of the data from the latitudinal chain of stations on the ground to reconstruct high-resolution latitude variations that would have been observed just below the current layer (Mersmann et al., 1976). A positive X-component (northward) is a response to an eastward current. If the magnetometers are responding to a Hall current in the E-region (i.e. if horizontal stratification of conductivities can be assumed), this corresponds to a westward convection velocity in the F-region. Note that the yellow and red colours reveal positive $B_X{}'$ (eastward current), whereas green and blue reveal negative $B_X{}'$ (westward current). Parts (a), (b) and (c) of Fig. 8 give the lagged (by 75 min) variations of the IMF components in the GSM reference frame. The dashed lines give the events identified in Fig. 6. The horizontal line is the latitude of the field-aligned ESR beam. Note that all events were seen while the IMF was southward.

Between 8:00 and 8:25 (roughly 10:45–11:10 MLT), weak westward current was seen poleward of a stronger eastward current. In this interval, the lagged IMF was strongly southward with a weak negative B_Y component. Thus, this is consistent with the magnetometer chain spanning the convection reversal of the dawn cell for IMF $B_Y < 0$. Note that the currents were not steady – 5 enhancements seen in the eastward current during this 25 min. In this interval, events 5a, 5b and 6 were identified from the radar data, however, no clear correspondence with the $B_X{}'$ variations is apparent.

Between 08:25 and 09:30, $B_X{}'$ oscillated between this situation (westward current poleward of eastward current) and the reverse situation (eastward current poleward of westward current). The latter is consistent with the chain straddling the convection reversal of the dawn cell for IMF $B_Y > 0$. The IMF data reveal several reversals of the polarity of IMF B_Y in this interval. For 09:03–09:19, the current is eastward at all latitudes, consistent with the chain moving into the dusk cell for IMF $B_Y > 0$. The plasma concentration (N_e) enhancement events seen by the ESR in this interval can all be associated with either oscillations in the form of the $B_X{}'$ latitude variation or with a transient enhancement of $B_X{}'$. Thus, there is structure in the detected currents that is broadly associated with the N_e events, although the association is not straightforward since the $B_X{}'$ signatures have a variety of forms. This is perhaps not surprising considering the variations in IMF B_Y and B_Z (Fig. 3), and the effects this will have on $B_X{}'$. In addition, the competing effects of magnetosheath precipitation, the enhanced loss rates associated with ion-neutral frictional heating and the effect of event evolution (Lockwood et al., 2000) will introduce variations into the form of the N_e events; this fact is reflected in the range of behaviours of T_e, $[T_i]_\parallel$ and $V_\parallel$ during the N_e enhancements.
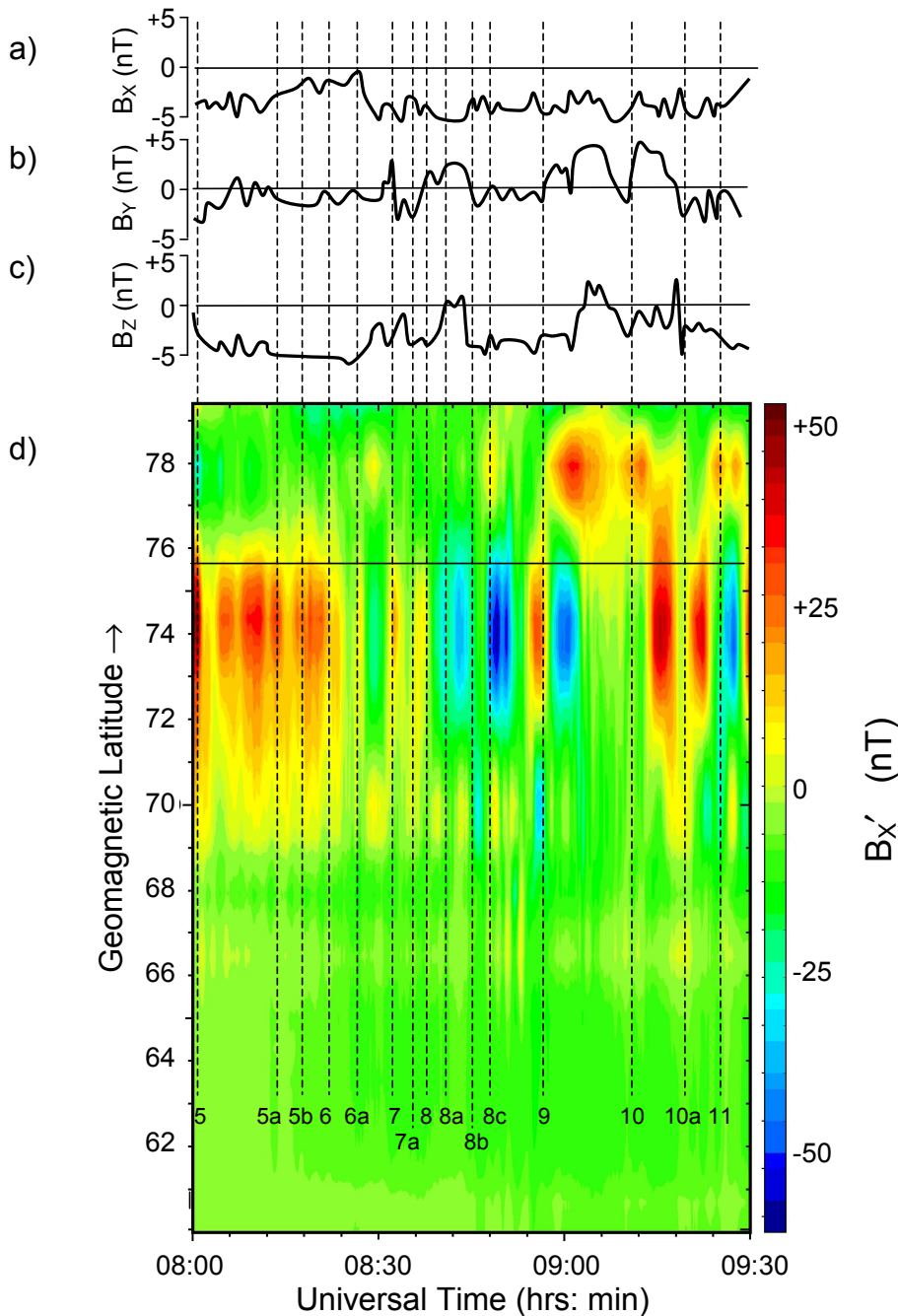
Fig. 8. **(a)** to **(c)**, the lagged (by 75 min) variations of the IMF components B_X, B_Y and B_Z in the GSM reference frame. **(d)** the "upward continuation" of the X component of the magnetic field, $B_X{'}$, as a function of latitude from the IMAGE magnetometer chain. The technique used to derive $B_X{'}$ employs Fourier analysis of the observations of the data from the latitudinal chain of stations on the ground to reconstruct high-resolution latitude variations that would have been observed just below the current layer. The vertical dashed lines give the times of the peaks in the N_e events defined in Fig. 6.

2.5 Convection observations

Figure 1 shows a 5-min integration convection pattern in an invariant latitude (Λ), with the MLT frame at 09:05. This has been derived by the AMIE technique, employing magnetometer, SuperDARN, DMSP and ESR observations. This is the time of the closest approach of the DMSP-F12 satellite to the ESR and marks the start of the cusp intersection (cusp ions are seen at 09:05–09:07 and the electron edge is encountered three times during the interval 09:07–09:08). The flows show a southward IMF flow pattern, with a transpolar voltage of 54 kV. A similar value for the transpolar voltage and flow

pattern is obtained for this time using model fitting to Super-DARN line-of-sight velocity data (Ruohoniemi et al., 1989, Ruohoniemi and Baker. 1998). The flow in the cusp region is directed towards dawn (westward), which is characteristic of a positive IMF B_Y for these northern hemisphere data (e.g. Heelis et al., 1984). With the inferred lag of 75 min for this interval, the relevant IMF data were recorded by ACE at 7:50. Figure 3 shows that the IMF B_Y component in GSM was indeed positive at this time, with negative IMF B_Z. At other times in interval A, the IMF B_Y was weakly negative and then the flow streamlines in the dayside polar cap were close to poleward with only a small eastward component. At such

times, the flow streamlines that passed over the ESR were closer to Cluster than seen in Fig. 1, in which the path of the DMSP-F12 satellite in this (Λ) - MLT frame is also plotted. The thicker segments of the path mark where the DMSP-F12 was in the dusk auroral oval (observing a sunward flow) and in the cusp (observing a structured anti-sunward flow). While within the polar cap, between these two segments, DMSP-F12 observed weak anti-sunward flow (see Fig. 4). The flows are consistent with the inference from the upward continuation magnetic disturbance, $B_X{}'$, as plotted in Fig. 8, with an eastward current at all latitudes showing that the magnetometer chain is in the dusk convection cell at this time. However, the $B_X{}'$ variation before and after the pass reveals the chain moving out of, and then back into a dawn cell. This is consistent with the zero-potential contour between the two cells lying close to the meridian of Svalbard, as seen in Fig. 1, where the locations of the two ESR beams can also be seen. Convection is poleward, consistent with the poleward phase motion of the events, but at this time, it has a westward component that is of the same order of magnitude as the poleward flow.

Figure 9 summarises some of the line-of-sight flow observations made on the dayside at a 2-min resolution by the SuperDARN radars. Each part shows a map of the dayside in geographic coordinates with noon at the top and the day-night terminator as shown. The vectors shown point along the beams where scatter was observed, and they have a length and polarity that is scaled according to the line-of-sight velocity. They are also colour-coded according to the magnitude of the observed line-of-sight velocity. Note that these are not 2-dimensional convection vectors. The DMSP-F12 pass is shown in the same format as Fig. 1, with the addition of a red arrow that gives the location of the satellite at that time. The yellow dot is the field-aligned ESR beam. At 09:01 UT (Fig. 9a), enhanced flows are seen in the polar cap (in red) and this patch subsequently migrates anti-sunward and fades in magnitude and size. A small patch of enhanced poleward flow is seen around the ESR. This has faded by 09:05 (Fig. 9b) but another patch to the west of the radar has appeared by 09:09 (Fig. 9c). This subsequently spreads eastward over the ESR (09:17, Fig. 9d). Note that the lagged IMF data shows positive IMF B_Y for almost all of the interval covered by Fig. 9 (Fig. 3) and the vector flow in the cusp is correspondingly westward (Fig. 1). Thus, the eastward expansion is not due to the curvature force on newly-opened field lines and is likely to reflect an eastward expansion or motion of the reconnection X-line. A decay in this enhanced flow starts near noon and spreads both east and west, such that by 09:21 (Fig. 9e), the enhanced flows are seen only in the mid-morning and mid-afternoon sectors. This behaviour is as predicted by Lockwood (1994) for an active X-line that forms near noon and then expands and bifurcates, giving active segments travelling toward both dawn and dusk. The data also reveal a convection reversal boundary (CRB), seen as a reversal of the line-of-sight flow from toward to away from the radar. This is near 75° in the morning sector and close to the satellite pass in the afternoon. By 09:27 (Fig. 9f),

the enhancement is not seen at all, and the CRB has migrated poleward in the morning sector, but not in the afternoon sector.

2.6 Global auroral observations

The flow streamlines in Fig. 1 are superposed on the relevant global auroral image taken by the Wideband Imaging Camera (WIC) of the FUV instrument on the IMAGE spacecraft (Mende et al., 2000). This imager covers the ultraviolet range of wavelengths between 140 and 180 nm with temporal resolution of 2 min. The original image was taken from a geocentric distance of 50 200 km and was remapped to a local time and geomagnetic latitude grid. The UV aurora is primarily observed in the regions of upward field-aligned current associated with the pattern of convection (the region 2 at dawn, on the equatorward edge of the convection boundary, and the region 1 at dusk, close to the convection reversal boundary). The DMSP-F12 satellite is poleward of the auroral oval when in the region defined as the polar cap from the precipitation characteristics.

The WIC camera is primarily sensitive to aurora created by electron precipitation, which when measured by DMSP in the cusp, showed very low characteristic energy (below 300 eV) and when combined with the small differential energy flux, this precipitation only produced a very weak signal from the cusp region. Even the electron precipitation measured by DMSP at around 09:09 with higher characteristic energies (several keV) was not intense enough and a gap appeared in the dayside aurora. The FUV instrument on IMAGE also contains the Spectrographic Imager (SI12) channel, which measures the Doppler shifted Lyman-alpha emission from precipitating protons (Mende et al., 2000). This imager is sensitive to emission from protons with at least 2 keV energy. The high energy tail of the differential ion energy flux (primarily protons) measured by DMSP created only a very weak signal in the proton aurora imager from the cusp (not shown). At the first crossing of the auroral oval by DMSP at about 71° magnetic latitude and 17:00 MLT (see Sect. 2.2), the UV images confirm the location of the proton precipitation equatorward of the most intense inverted V-like electron precipitation.

2.7 Cluster observations

Figures 10b to 10e shows plasma observations made during interval A by the Cluster spacecraft, and Fig. 10a reproduces the N_e variation shown in Fig. 6a, shifted in time to obtain the best agreement (see below). Figure 10b shows the spacecraft potential from the EFW instruments on all 4 spacecraft, a measure of the plasma concentration around the spacecraft. The spacecraft potential was held almost constant by the ASPOC instruments which were active on spacecraft C3 and C4. However, close inspection revealed that for this case with very low ambient plasma concentrations, the potential of C3 and C4 still varied about the almost constant value due to the ambient plasma concentration variations. Cross-
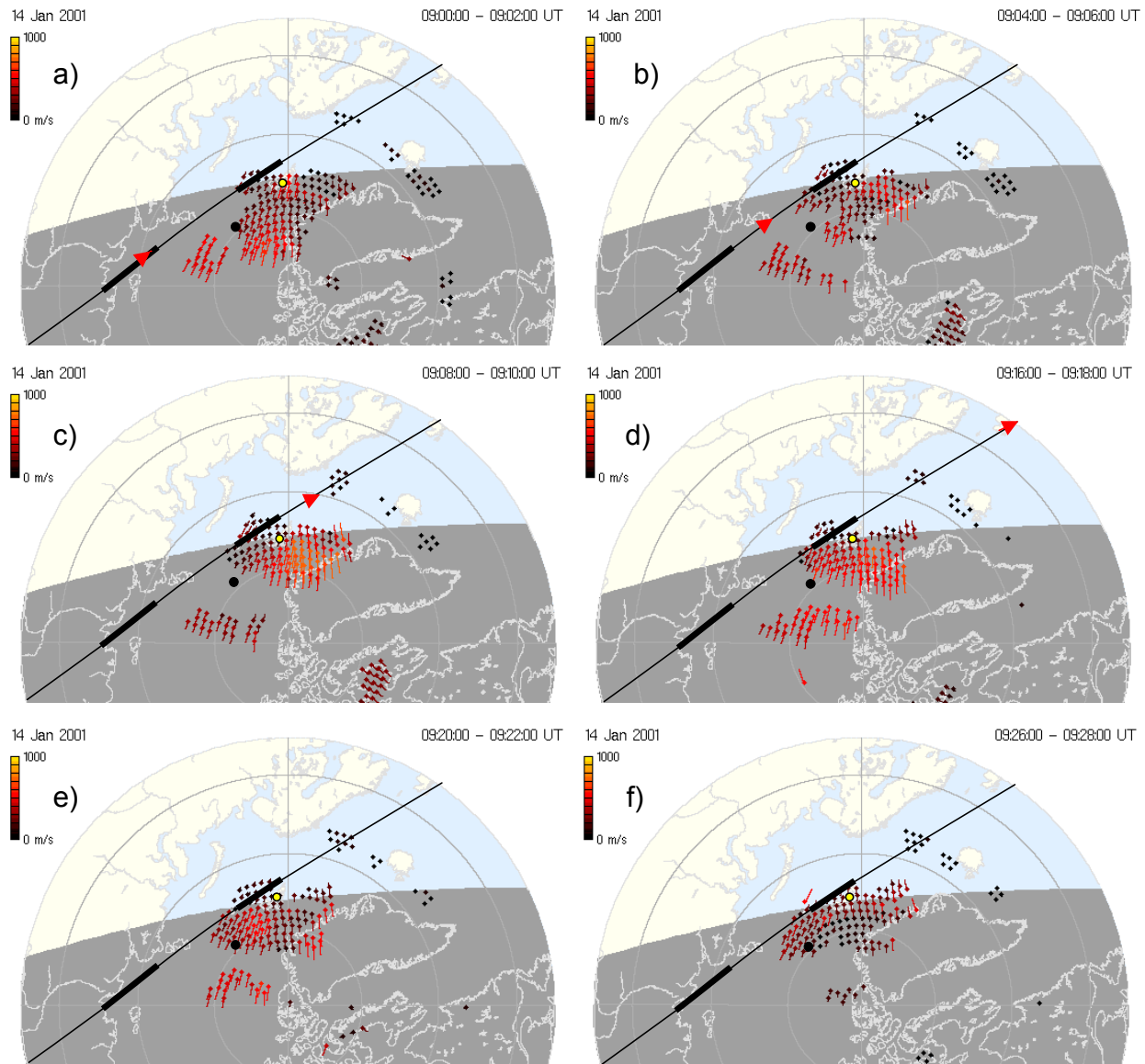
Fig. 9. SuperDARN observations of the line-of sight plasma velocities seen at 09:00–09:30. Selected frames are for 2 min scans centred on: **(a)** 09:01, **(b)** 09:05, **(c)** 09:09, **(d)** 09:17 **(e)** 09:21, and **(f)** 09:27. The orbit of DMSP-F12 is shown in each case, with the auroral oval and cusp locations marked: the red arrow gives the location of the satellite in each case. The ESR field-aligned beam is shown as a yellow dot.

correlation of the potential values seen on these spacecraft (C3 and C4) with an average of those seen by C1 and C2 (on which ASPOC was off) showed a systematic variation with only small scatter. Fitting the scatter plot with an exponential variation gives an excellent fit in both cases and this was used to scale the data by C3 and C4, taken with ASPOC turned on, into the values that would have been seen had ASPOC been turned off. Fig. 10b shows that the four spacecraft saw fluctuations in the plasma concentration in roughly 10-min time scales (9 in 90 min) that were almost identical, indicating that the plasma structures were considerably larger than the inter-craft separations of the order of 600 km.

Parts (c) to (e) of Fig. 10 analyse the nature of these plasma

concentration structures using data from spacecraft C3. Figures 10c and 10d show the data from the LEEA and HEEA detectors on the PEACE instrument, respectively. In both cases, the particles seen are in zone 11 of the detector, which makes continuous observations of electrons moving in the $+Z_{GSE}$ direction. The ASPOC instrument held the spacecraft potential such that the photoelectrons were seen by LEEA up to only 10 V (photoelectrons seen by the spacecraft with ASPOC turned off extended up to about 30 eV in the LEEA data). Fig. 10e shows the ion observations made by the CIS instruments on board C3 (Rème et al., 1997, 2001, this issue). Increases in the fluxes of ions and high-energy electrons were seen co-incident with the low-energy electron in-
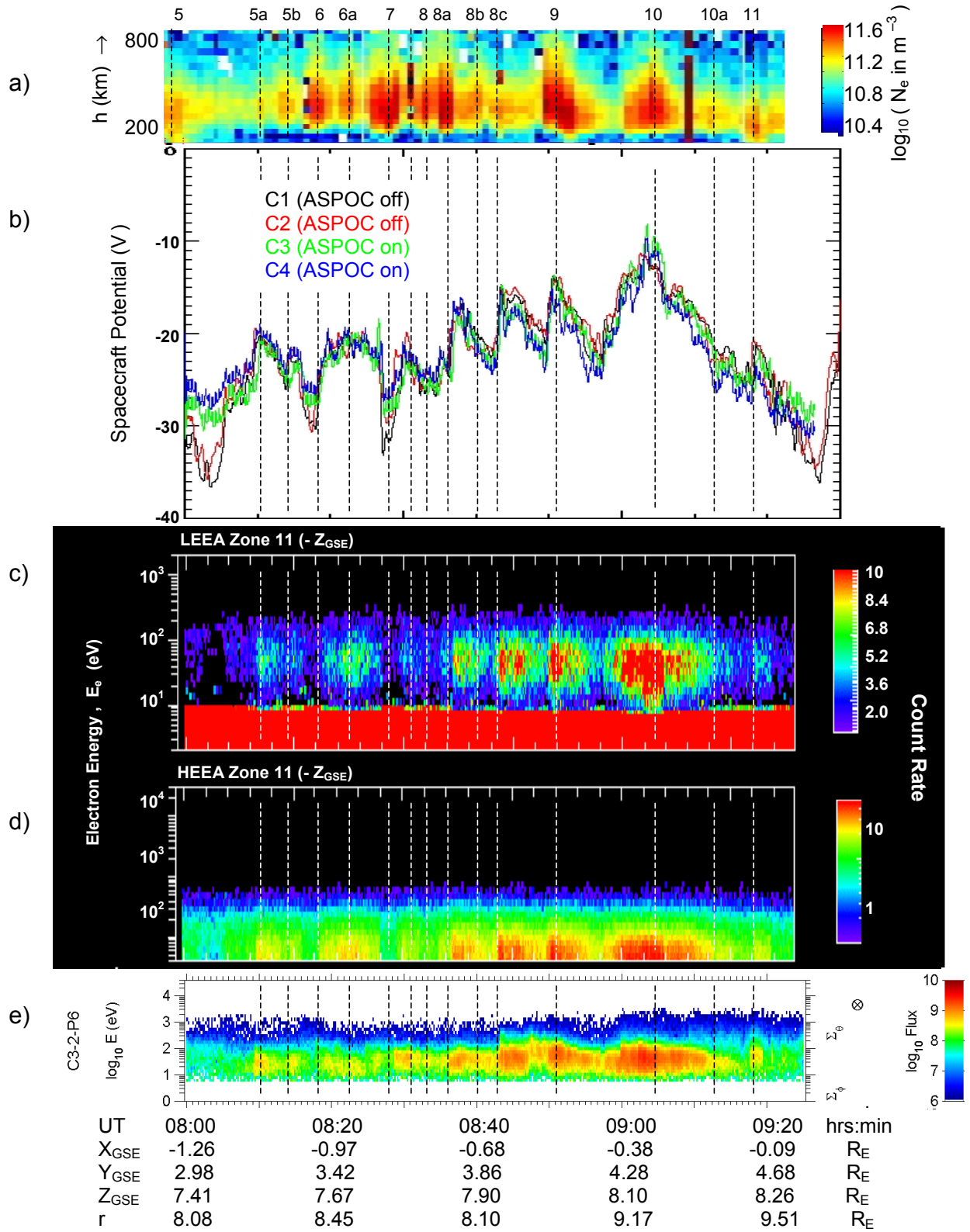
Fig. 10. From top to bottom: **(a)** the electron concentration observations by the field-aligned ESR beam, as shown in the top panel of Fig. 6, but shifted to earlier times to make events 5 and 11 agree. **(b)** potential measurements for all 4 spacecraft from the EFW instrument. **(c)** electron observations made by the HEEA detector of the PEACE instrument on the Cluster spacecraft 3 (C3); **(d)** electron observations made by the LEEA detector of the PEACE instrument on C3. In both (b) and (c), the particles seen are in zone 11 of the detector, which makes continuous observations of electrons moving in the $+Z_{GSE}$ direction. **(e)** ion observations made by the CIS instruments on board Cluster C3.

creases. Events in both ion and electron data show relatively sudden onsets, followed by a slower decay. Figure 10c shows that the fluxes of lowest energy magnetosheath electrons seen by LEEA (10–30 eV) are quite strongly modulated during the events, and the lowest energy at which significant fluxes of such electrons are seen falls as the plasma concentration rises.

In comparing the plasma concentration structures seen by the ESR and by the Cluster spacecraft, several points must be remembered. In the 1.5 hours shown, the ESR moves in MLT from near 10:45 to 12:15, while Cluster remains close to 15:00 MLT. Conversely, the ESR remains at an invariant latitude of 75.1°, while Cluster moves from near 85° to 79°. Thus, the separation of the two decreases by 1.5 hours in MLT and by about 6° in invariant latitude. Thus, we do not expect the propagation delay of any events that pass over both to be constant, although it might vary approximately linearly. Second, Cluster traverses much of the mantle in this period and plasma concentrations increase correspondingly, whereas the difference in latitude between the ESR and the open-closed boundary does not appear to drift very much. Thus, it is not surprising that events become successively larger in amplitude in the Cluster data, but this trend is not found in the ESR data. In Fig. 10, the ESR data have been shifted forward in time by a lag that varies linearly with time. The end of event 5 is matched up to the end of an event at 08:00 in the EFW data, and the small event 11 is matched up to the small event in the EFW data. This yields a lag of 150 s at 08:00 and a lag of 244 s at 09:00 and gives an excellent match for events 9 and 10 in the Cluster data, and events 8a and 7 are seen in the Cluster data but the lag appears to be slightly overestimated. Between events 8c and 9 is an event seen by EFW, but absent in the ESR data; however, inspection of Fig. 6 reveals that $[T_i]_\parallel$ is strongly elevated at this time, indicating that the ionospheric enhancement may have been countered by enhanced plasma loss rates due to the fast plasma flow. Similar considerations apply to the minima between events 7 and 8 and between events 6a and 7, and agreement for events 6a to 8 is not very close.

The centre times of the ESR events are marked with dashed lines, as in Figs. 6 and 8. Given the changing separation between ESR and Cluster, and the complications associated with flow enhanced ionospheric loss rates, the data suggest a surprising correspondence between the two data sets.

3 Discussion

The period studied here (08:00–09:30) reveals a series of events with a repeat interval of the order of 10 min in a variety of data sets. Higher resolution data reveals further (smaller) events providing a repeat period of about 6.5 min. These values are similar to the average for the distribution of repeat periods for dayside auroral transients (Fasel, 1995), magnetopause FTEs (Lockwood and Wild, 1993), poleward-moving cusp/cleft flow channels seen by HF radar (Provan

and Yeoman, 1999; McWilliams et al., 2000) and polar cap patches (Sojka et al., 1994). Thus, they are consistent with a characteristic quasi-periodicity that is seen throughout the region of dayside open field lines (cusp/cleft, mantle and polar cap). The pass of the DMSP-F12 satellite around 09:05 UT reveals that the cusp and the electron edge were equatorward of both ESR radar beams, which were both on open field lines. Events were seen in the ionospheric plasma density in both beams; they were moving poleward along the low-elevation beam and by mapping these back in latitude when the IMF was southward confirms that the same events were seen as they passed through the field-aligned beam. Comparison with high-resolution magnetometer data indicates that there are associated changes in ionospheric currents and convection, but these vary in their nature, almost certainly due to changes in the IMF B_Y and B_Z. The events were seen by the ESR after only a very small lag following the corresponding enhancements of electron (and to a lesser extent ion) concentrations in the mantle region of the tail lobe, as monitored by Cluster. The surprising result, therefore, is that there appears to be signatures of polar cap patches in the tail lobe particle populations, as well as in the ionosphere.

3.1 IMF control of events

Figure 3a shows that the IMF at ACE was predominantly southward until 09:45, and we can identify the effects of the northward turning at this time with the change in the ground-based magnetometer data (as shown in Fig. 3b for the IMAGE chain, but also found in the Greenland magnetometer chain) at 11:00, consistent with the inferred propagation lag of 75 min at this time. The SuperDARN radar network also revealed a drop in the transpolar voltage following the northward turning (Fig. 3i). Thus, the events seen by the ESR before 11:00 are for predominantly southward IMF conditions. Brief periods of northward IMF were seen at ACE at 07:29–07:32 and 07:51–07:54 which applying the 75 min lag gives times of 08:44–08:47 and 09:06–09:09. These intervals do not appear to change the occurrence of the events seen by the radar; however, at these times, between events 6 and 8, there is a marked slowing in the phase speed of the poleward motion of the events. This is clearly reflected in the phase velocity of the poleward motion of the events, V_e (Fig. 6). Although event velocities do generally decrease following the arrival of northward IMF turnings at 08:45 and 10:45, there is no good overall correlation with IMF B_Z. The IMF B_x was negative throughout interval A, with B_Y negative for the majority of the interval (between -3 and -1 nT) with a few excursions to positive B_Y (to about $+4$ nT).

Strong ion-neutral frictional heating (high $[T_i]_\parallel$) is seen between some of the enhanced plasma concentration N_e events, in particular, between events 6a and 7, 7 and 8, and 8c and 9. Figure 8 shows that these are associated with changes in the direction of the east-west current, as inferred from the upward continuation northward magnetic field $B_X{}'$, which, in turn, can be associated with changes in the polarity of the IMF B_Y component.

3.2   Implications for the causes of the polar cap patches

The source of F-region polar cap patches has been a subject of considerable debate (e.g. Rodger et al., 1994a, b, c; Lockwood and Carlson,1992, 1994; Ogawa et al., 2001). Several classes of theory have been proposed:

(1) the density could be enhanced by the magnetosheath particle precipitation (Whitteker, 1977; Watermann et al., 1992), such that the plasma concentration depends on the time elapsed since the field line was reconnected. In such cases, patches may be seen at one point, but only if the elapsed time since reconnection of the field lines monitored varied quasi-periodically (Davis and Lockwood, 1996). This does not give an explanation of the minima seen between events by imagers, meridian scanning photometers and HF backscatter radars;

(2) the minima between patches could have been produced by channels of enhanced flow which raise the plasma loss rate (Rodger et al., 1994a, c; Balmforth et al., 1998, 1999) or by

(3) a hardening of the electron precipitation spectrum in regions of upward field-aligned current (Lockwood et al., 1993a, 2001b; Davis and Lockwood, 1996);

(4) the enhanced plasma within patches could be produced by solar EUV radiation in the sunlit sub-auroral region and moved into the polar cap by time-varying convection in response to reconnection pulses (e.g. Lockwood and Carlson, 1992), in which case, the minima are due to the relative absence of that photoionisation in the history of some flux tubes;

(5) Lockwood et al. (2000) recently used a combination of three of these models to explain some patches seen using the ESR, the Cutlass radars and optical instruments; a large longitudinal extent of the reconnection site was an important part of this explanation.

Model (1) predicts that the F-region plasma concentration, N_e, and the electron temperature, T_e, will be enhanced together when they first form (this is not true further into the polar cap because enhanced N_e persists, but T_e decays rapidly when the magnetosheath electron precipitation decays away; see Watermann et al., 1992, 1994; Davis and Lockwood, 1996). Model (2) predicts that high ion temperatures (including $[T_i]_\parallel$) will be found within the gaps between the events of higher N_e, at least where the gaps first form. (Again, further into the polar cap, enhanced $[T_i]_\parallel$ would decay if the fast ion flows decay, but low N_e would remain as a fossil of the remnant of the flow bust; see Balmforth et al., 1998, 1999). Model (3) predicts enhancements in the E-region below the F-region depletion and, like model (1), predicts that N_e and T_e in the F-region will rise and fall in unison. Model (4) predicts that T_e will fall where N_e rises, since the same downward heat flux is shared among more ionospheric particles. The ESR data shown in Fig. 6 offers some support for several of these concepts. First, when the IMF

is southward, both T_e and N_e in the F-region are enhanced along the field-aligned ESR beam, showing the presence of soft, magnetosheath-like electron precipitation. (This should be compared with the situation after 11:15 when the IMF is generally northward and the cusp/LLBL precipitation is poleward of the Longyearbyen field line, making both T_e and N_e lower; see Opgenoorth et al., 2001, this issue). More obvious structure is seen in N_e than in T_e, but this is consistent with the modelling of Davis and Lockwood (1996) for a radar location that is not too close to the open-closed boundary but still within the cusp region. These events, like those reported by Ogawa et al. (2001), do not show an association with rises in $[T_i]_\parallel$. However, other events do show strongly enhanced $[T_i]_\parallel$ in the N_e minima between two events. In fact, the absence of such a rise in $[T_i]_\parallel$ is not inconsistent with model (2) since the rapid flows causing the heating could have subsided, leaving a "fossil" trough between events. Third, there are some cases in which there are minima in T_e coincident with the peaks in N_e and the changes in the flow that one needs to invoke patches of enhanced N_e are seen to be present in the high resolution magnetometer data.

Figure 10 indicates that the patches seen in the high-altitude mantle (at geocentric distance of about $10\,R_E$, see Fig. 1) may be closely related to the ionospheric N_e patches. The repeat periods are similar in the two datasets and, with the inclusion of a small but variable lag, we can make an association between the two sets of data in those cases where flow changes do not appear to be a major factor. This poses interesting new questions for the models of patch production. In particular, the enhancements seen by the ESR at the greatest altitudes appear to be related to variations in the flux of the softest electrons. This strongly implies that these patches were produced by modulations in the precipitation magnetosheath electrons.

An important point is that the ESR and Cluster are well separated at this time. Thus, if the relationship implied by Fig. 10 is real and events do indeed pass over both, this requires that the events be large (covering over 4 hrs of MLT, i.e. > 1200 km). For the flow pattern shown in Fig. 1, it is certainly possible that events formed along the afternoon sector open-closed boundary could pass over the Cluster and ESR field lines at similar times (the best-fit lag in Fig. 10 is 2.5 min at 08:00 and 4 min at 09:00). Second, if the variations in the precipitating magnetosheath electron flux are a contributory cause of the patches, then they cannot be a function of elapsed time since reconnection, as this would yield a relatively static region of enhanced N_e through which newly-opened field lines convect. Rather, the convection of patches into the polar cap with the newly-opened field lines requires that the electron flux enhancement persists on some field lines (i.e. within the patch) but is always absent from others (i.e. in the gap between patches).

Thus, the variations could be caused by the concentration variations in the source magnetosheath plasma, giving rise to variations in the fluxes injected into the magnetosphere. This being the case, polar cap patches would be seen if the reconnection was steady or pulsed, and flux increases would

be seen in both injected ions and electrons. The CIS data do reveal changes in the fluxes of the magnetosheath ions during this period, although they are not as distinct as in the low-energy electron data and a one-to-one correspondence is not always found. Furthermore, this mechanism does not explain the cusp ion steps and the transient changes in the flow seen by the SuperDARN HF radars and the magnetometers. Thus, magnetosheath plasma concentration fluctuations are, at most, only a partial explanation.

A key unanswered question in understanding the behaviour of the electron gas relates to how the observed quasi-neutrality is maintained along newly-opened field lines on which magnetosheath and magnetospheric plasma is mixing after reconnection (Burch, 1985). Several authors have found evidence for a potential barrier at the magnetopause that appears to hold back the lowest energy magnetosheath electrons (Wing et al., 1996; Lockwood and Hapgood, 1997, 1998). Furthermore, electrons appear to undergo an unexplained heating when crossing the magnetopause along open field lines (Onsager et al., 2001) and the mirrored part of the bi-directional streams of strahl electrons in the magnetosphere does not appear to escape back into the magnetosheath across a magnetopause, even where the magnetopause is known to be a rotational discontinuity threaded by the field lines (Shirai et al., 1998). These various clues point to a process that modulates the magnetosheath electron flux and spectrum as it enters the magnetosphere and this may be relevant to the low-energy electron flux variations shown in Fig. 10.

3.3 The role of pulsed magnetopause reconnection

Both the electron and ion dispersion data from the DMSP-F12 pass reveal the effects of pulses in the magnetopause reconnection rate. The electron observations reveal motions of the open-closed boundary between 09:07 and 09:08 that are consistent with a reconnection pulse and the structure in the ion dispersion reveals that there were other reconnection pulses prior to this. The evolution of a stepped dispersion to a sawtooth dispersion is consistent with an increase in the amplitude of the reconnection pulses (Morley and Lockwood, 2001). Parts (a) and (b) of Fig. 11 summarise the location of DMSP-F12 relative to the ESR showing, respectively, the invariant latitude and the MLT of both for the cusp intersection. Figure 11c gives the cutoff velocity of the precipitating magnetosheath ions, V, defined from the differential energy flux contour of 10^8 cm^{-2} sr^{-1} s^{-1} (separating yellow and green in the spectrograms shown in Fig. 4). The events defined in the incoming magnetosheath ions, separated by steps and/or gaps are labelled I1, I2, I3, I4 and I5 and the event seen in the departing BPS electrons is labelled E.

The satellite entered event I1 at 09:05:10 UT, when DMSP-F12 was at $\Lambda = 75.85°$ and an MLT of 13:46 hrs. This is (to within the ESR data resolution) at the same time that the ESR entered event 10, but at a slightly higher latitude than the ESR (which was at $\Lambda = 75.1°$). However, the ESR was at an MLT 1.82 hours smaller than that of the satel-

lite, and a small angle of the event boundary with respect to the L-shells (of $\delta\Lambda_1$ of 0.41° per 1 hr of MLT), would mean that DMSP-F12 and the ESR entered the same event at about the same time, provided that the event is at least about 2 hrs of MLT in longitudinal extent. Upon entering the event, DMSP-F12 saw the onset of much more enhanced (and highly structured) fluxes of magnetosheath electrons; these persisted until the satellite moved through the equatorward edge of ion event I4. This happened at 09:06:39, when DMSP-F12 was at $\Lambda = 74.28°$ and an MLT of 12:29 hrs (only 0.52 hrs greater than the MLT of the ESR). If the events were L-shell aligned, this yields a combined latitudinal width of events I1, I2, I3 and I4 of $\delta\Lambda = 1.57°$, corresponding to about 188 km at 300 km altitude. However, the satellite has moved through 1.3 hrs in MLT, and thus, $(1.3\delta\Lambda_1) = 0.53°$ of this latitude difference can be attributed to the orientation of the events, giving a corrected $\delta\Lambda$ of 1.04° (corresponding to 126 km). Figure 7 gives a poleward phase motion of event 10 of 300 m/s, and at this speed, the combined events I1-I4 would pass over the field-aligned ESR beam in 420s and the ESR would therefore exit from them at 09:12:00. This is exactly when event 10 ceases and thus, we can associate the combined cusp ion events I1-I4 with the ESR event 10. The fine structure in the DMSP-F12 ion data cannot be detected in the ESR data, which thus appears as one single event. However, the ESR did detect a drop in electron temperature in the first half of event 10 that can be associated with a drop in magnetosheath electron precipitation seen by DMSP-F12 within event I1.

The small detached ion event I5 was seen at 09:07:05 when DMSP-F12 was at $\Lambda = 73.5°$ and at an MLT of 12:15 hrs. Using the poleward event phase speed of 300 m/s (Fig. 7), this event would arrive at the ESR field-aligned beam at 09:17:24, a predicted time which lies within the interval 09:16:00–09:18:00 when event 10a was observed by the ESR. Thus, we can associate the ion step I5 with ESR event 10a.

The DMSP-F12 electron data shows a rapid reconnection pulse giving rise to the dispersed loss of energetic BPS electrons in event E between 09:07:27 and 09:08:02, when DMSP-F12's (Λ, MLT) coordinates are 72.5°, 12:04 hrs and 71.6°, 11:28 hrs, respectively, and the ESR's are 75.1°, 11.97 hrs and 75.1°, 11.98 hr. Thus, the satellite detected the edges of event E at $\Delta\Lambda$ of 2.6° and 4.5° equatorward of the ESR and at almost same MLT. Figure 7 shows that event 11 moved poleward at about 390 m/s and, at this poleward phase speed, the edges of this event would have reached the ESR after delays of 773 s and 1338 s, i.e. at 09:20:20 and 09:30:20. Figure 6 shows that this is when event 11 was seen in the ESR field-aligned beam. Thus, we can firmly identify the electron event E seen by DMSP-F12 with event 11 seen by the ESR. Thus, the data are fully consistent with the idea that the N_e enhancements seen by the ESR, at least during the cusp pass by DMSP-F12, correspond to the features of the satellite pass that can be attributed to pulsed reconnection.
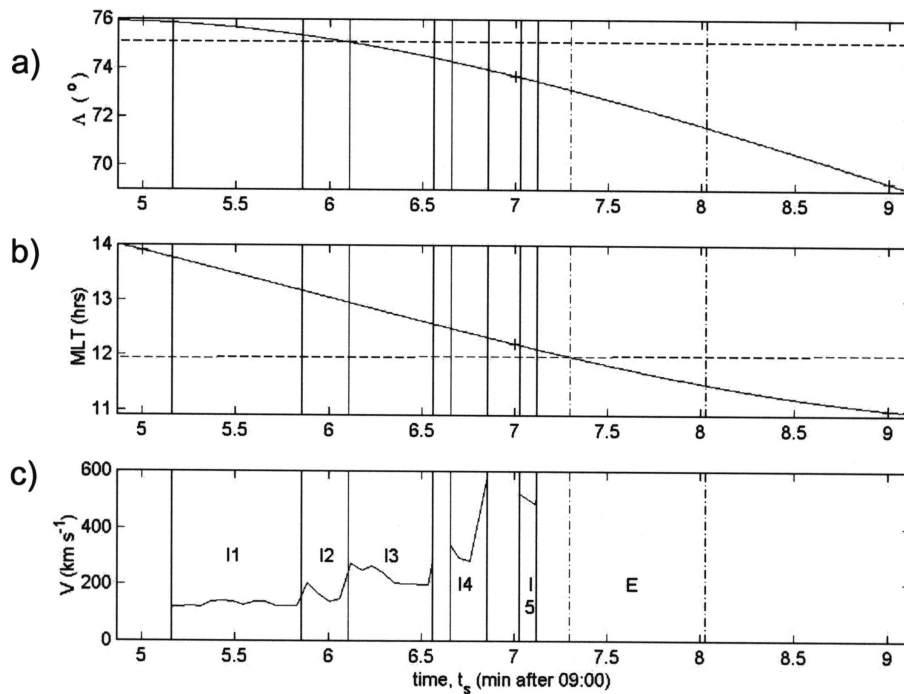
The flows seen by the SuperDARN radars are enhanced

Fig. 11. **(a)** The invariant latitude (Λ) and **(b)** the Magnetic Local Time (MLT) of the DMSP-F12 satellite during the cusp intersection. The corresponding values for the ESR field-aligned beam are given by dashed lines and the crosses refer to the tick marks on the relevant section of the spectrograms shown in Fig. 5. **(c)** the cutoff ion velocity, V, of cusp ions. Ion events between steps I1, I2 and I3 are contiguous, whereas I4 and I5 form isolated patches. The dispersed disappearance of BPS electrons is labelled as event E.

poleward of the ESR in the interval 09:09–09:19 (Fig. 9), whereas event 10 is seen at the ESR field-aligned beam at 09:05–09:12. Thus, we can also associate the flow enhancement shown in Fig. 9 with event 10 seen by the ESR and with the combined cusp ion events (I1-I4) seen by DMSP-F12, but the inductive smoothing of the flow, relative to the reconnection rate pulse means that its onset is delayed and its duration increased. Both the onset and decay of the flow event imaged by SuperDARN spreads towards dusk over the ESR; this is despite the fact that the relevant IMF B_Y is positive (Fig. 3) and the associated Svalgaard-Mansurov effect provides flow in the cusp toward dawn (Fig. 1). This supports the concept of a propagating active reconnection line around the afternoon sector away from noon and, in this case, towards dusk, as discussed by Lockwood et al. (1993c), Lockwood (1994), Milan et al. (2000) and McWilliams et al. (2001a, b).

4 Concluding comments

Figure 12 (adapted from Lockwood, 1994) shows schematically newly-opened field lines evolving away from a site X at which the reconnection rate is pulsed. On the left is a noon-midnight cross section of the magnetosphere, viewed from dusk and with the Sun to the left. X is a low-latitude reconnection site (between the magnetic cusps) converting closed field lines (c, such as field line 1) to open ones (o, such as 2–5) by reconnecting them with draped magnetosheath field lines (i). The reconnection is shown as having proceeded in two pulses, generating the corresponding bundles of newly-opened flux, shown as A and B. Since A was re-

connected before B, it has evolved further away from the nose of the magnetosphere. The magnetosheath plasma concentration and temperature fall with distance from the nose of the magnetosphere, and thus, field lines in A will be full of lower fluxes of magnetosheath particles flowing along the field lines across the magnetopause than will field lines in B, at the time shown. In addition, the faster tailward convection of the magnetospheric portion of flux tube A means that a smaller fraction of the injected population reaches the ionosphere. Thus, the fluxes of the precipitating magnetosheath particles fall with elapsed time since reconnection.

The right-hand figure is a view looking down on the dayside polar cap in the northern hemisphere, with noon to the top and dawn to the right. The footprints of the field lines shown in Fig. 12a are shown, following a convection flow streamline. Cusp ion steps form between events and propagate poleward with the convection velocity. The production of stepped and sawtooth ion dispersion signatures by different satellite passes through such patches has been discussed and modelled by Lockwood and Davis (1996) and Morley and Lockwood (2001). Observations of cusp ion steps reveal spatially contiguous patches of ion precipitation, such as predicted in Fig. 12 for A and B. However, auroral and radar signatures show that there are gaps between poleward-moving events. As discussed earlier, the origins of these gaps is still a matter of debate, but the data presented here imply that at least some of them may be caused by variations in the magnetosheath electron precipitation within the magnetosphere. Since these have been detected by Cluster above the auroral acceleration region, this is a separate effect from the electron
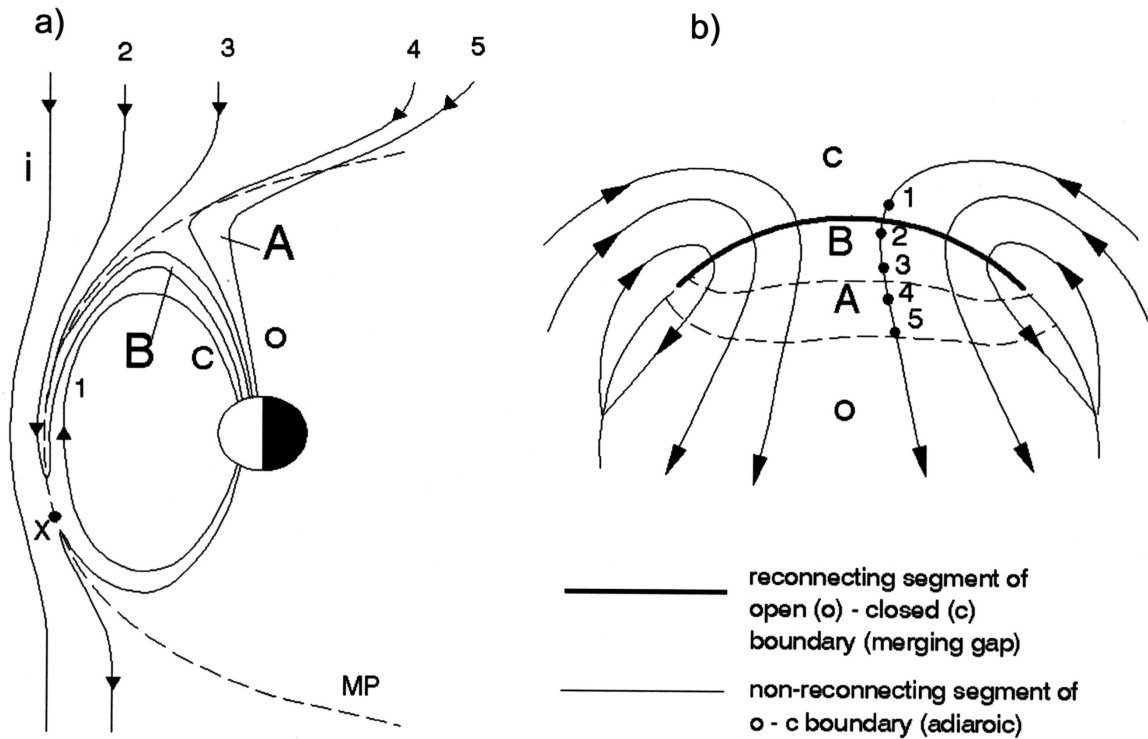
Fig. 12. (a) Schematic illustration of the dayside magnetosphere near the noon-midnight cross section of the magnetosphere, viewed from dusk and with the Sun to the left. X is a low-latitude reconnection site (between the magnetic cusps) converting closed field lines (c, such as field line 1) to open ones (o such as 2–5) that thread the magnetopause, the dashed line labelled MP, by reconnecting them with draped magnetosheath field lines (i). A and B are patches of newly-opened field lines produced by reconnection pulses at X. **(b)** The view looking down on the dayside polar cap in the northern hemisphere, with noon to the top and dawn to the right. The footprints of the field lines on the left are shown, following a convection flow streamline. The thick line is the ionospheric footprint of the reconnection line X

acceleration effect in regions of upward field-aligned current (model 3), as proposed by Davis and Lockwood (1996) and Lockwood et al. (1993a, 2001b).

As discussed above, as the newly-opened flux tubes evolve, the fluxes of the precipitating magnetosheath particles fall. Thus, variations in the flux and spectra of the injected magnetosheath ions and electrons observed by Cluster could be interpreted as variations in the elapsed time since reconnection. With this being the case, when Cluster was within region A, it would see lower fluxes that decayed further as the point migrated anti-sunward where the field lines observed thread the boundary. However, as a newer region B passes over the satellite, the point where the observed field lines thread the magnetopause jumps sunward and the satellite sees a sudden rise in fluxes and temperature. These then decrease again slowly, as for the prior event as it evolves anti-sunward. Thus, the variations seen by Cluster could be explained in terms of variations of the elapsed time since reconnection of the field lines sampled. This interpretation is essentially the same as that successfully applied to an FTE signature at the magnetopause (Lockwood and Hapgood, 1998), to the cusp ion structure at middle and low-altitudes (respectively, Lockwood et al., 1998 and Lockwood and Davis, 1996) and to the ESR concentration and

temperature variations (Davis and Lockwood, 1996).

However, the combination of Cluster and ground-based data presented here suggests that this is not the explanation of these Cluster data, or perhaps only a partial explanation. If the association of the electron flux enhancements seen by Cluster with the ESR patches is real, then the former should convect poleward into the tail lobe, mirroring the evolution of the ionospheric patches as they migrate poleward into the polar cap. In other words, they should maintain their relatively enhanced magnetosheath electron precipitation at all times as they move into the tail lobe. This means that the enhancements are not just reflecting variations in elapsed time reconnection and a significant additional mechanism is at work.

Figure 10 suggests that at the centre of patches, the plasma concentration in the F-region and in the topside ionosphere is enhanced by increased flux of the lowest energy magnetosheath electrons. If this is due to a lowering of a potential barrier at the magnetopause, then this feature must persist on certain field lines, but be absent at all times on others. One possibility is that the amplitude of the potential barrier presented to magnetosheath electrons is decreased where the magnitude of the boundary-normal magnetic field is increased. This would mean that patches of the enhanced boundary-normal field (produced by pulses of enhanced reconnec-

tion rate) would effectively be "holes" in the magnetopause that would allow lower energy magnetosheath electrons to enter the magnetosphere. Since these field lines maintain their enhanced boundary-normal field as they evolve into the tail lobe, the enhanced low-energy electron fluxes would then persist as the field lines evolve into the polar cap with increasing elapsed time since reconnection, giving a poleward-moving polar cap patch in the ionosphere.

We note that the association between the polar cap patches (seen by the ESR) and the plasma concentration enhancements (seen by Cluster) can only be made tentatively in this case. The problem is that the conjunction between the Cluster footprint and the ESR, at least as predicted by the magnetic field model, is not close. This means that changes in the speed and direction of convection result in large variations in the lag between the ESR and Cluster data. We intend to search for further examples in combined Cluster-ESR data, with closer conjunction of the two when located within the dayside polar cap. We also would like to find examples in which the convection flow pattern remains relatively constant, enabling us to distinguish the effects of modulations to the magnetosheath electron precipitation from the consequences of transient convection changes through flux tube evolution and enhanced loss rates.

References

Balmforth, H. F., Moffett, R. J., and Rodger, A. S.: Modelling studies of the effects of cusp inputs on the polar ionosphere, Adv. Space Res., 22(9), 1391–1394, 1998.

Balmforth, H. F., Moffett, R. J., and Rodger, A. S.: Localised structure ion the cusp and high latitude ionosphere, A modelling study, Ann. Geophysicae, 17, 455–462, 1999.

Burch, J. L.: Quasi-neutrality in the polar cusp, Geophys. Res. Lett., 12, 469–472, 1985.

Cowley, S. W. H. and Lockwood, M.: Excitation and decay of solar-wind driven flows in the magnetosphere-ionosphere system, Ann. Geophysicae, 10, 103–115, 1992.

Cowley, S. W. H., Morelli, J. P., and Lockwood, M.: Dependence of convective flows and particle precipitation in the high-latitude dayside ionosphere on the X and Y components of the interplanetary magnetic field, J. Geophys. Res., 96, 5557–5564, 1991a.

Cowley, S. W. H., Freeman, M. P., Lockwood, M., and Smith, M. F.: The ionospheric signature of flux transfer events, in "CLUSTER - dayside polar cusp", (Ed) Barron, C. I., ESA SP-330, 105–112, European Space Agency Publications, Nordvijk, The Netherlands, 1991b.

Davis, C. J. and Lockwood, M.: Predicted signatures of pulsed reconnection in ESR data, Ann. Geophysicae, 14, 1246–1256, 1996.

Escoubet, C. P., Smith, M. F., Fung, S. F., Anderson, P. C., Hoffman, R. A., Basinska, E. M., and Bosqued, J. M.: Staircase ion signature in the polar cusp: a case study, Geophys. Res. Lett., 19, 1735–1738, 1992.

Farrugia, C. J., Sandholt, P. E., Denig, W. F., and Torbert, R. B.: Observation of a correspondence between poleward-moving auroral forms and stepped cusp ion precipitation, J. Geophys. Res., 103, 9309–9315, 1998.

Fasel, G. J.: Dayside poleward moving auroral forms: a statistical study, J. Geophys. Res., 100, 11 891, 1995.

Foster, J. C.: Plasma transport through the dayside cleft: A source of ionisation patches in the polar cap, in: Electromagnetic coupling in the polar clefts and caps, (Eds) Sandholt, P. E. and Egeland, A., Kluwer, 343–354, 1989.

Foster, J. C. and Doupnik, J. R.: Plasma convection in the vicinity of the cleft, J. Geophys. Res., 89, 9107–9113, 1984.

Gosling, J. T., Thomsen, M. F., Bame, S. J., Onsanger, T. G., and Russell, C. T.: The electron edge of the low-latitude boundary layer during accelerated flow events, Geophys. Res. Lett., 17, 1833–1836, 1990.

Hapgood, M. A., Bowe, G., Lockwood, M., Willis, D. M., and Tulunay, Y.: Variability of the interplanetary magnetic field at 1 AU over 24 years: 1963–1986, Planet. Space Sci., 39, 411–423, 1991.

Heelis, R. A.: The effects of interplanetary magnetic field orientation on dayside high-latitude convection, J. Geophys. Res., 89, 2873, 1984.

Jenkins, B., Moffett, R. J., Davies, J. A., and Lester, M.: Nightside ion-neutral frictional heating: atomic and molecular ion temperature anisotropy and ion composition changes, J. Atmos. Sol-Terr. Phys., 59, 1329–1343, 1997.

Karlson, K. A., Øieroset, M., Moen, J., and Sandholt, P. E.: A statistical study of flux transfer event signatures in the dayside aurora: the IMF B_Y-related postnoon-prenoon asymmetry, J. Geophys. Res., 101, 59–68, 1996.

Kuo, H., Russell, C. T., and Lee, G.: Statistical studies of flux transfer events, J. Geophys. Res., 100, 3513–3519, 1995.

Lockwood, M.: Ionospheric signatures of pulsed magnetopause reconnection, in: "Physical signatures of magnetopause boundary layer Processes", (Eds) Holtet, J. A. and Egeland, A., NATO ASI Series C, Vol. 425, Kluwar, 229–243, 1994.

Lockwood, M.: The relationship of dayside auroral precipitations to the open-closed separatrix and the pattern of convective flow, J. Geophys. Res., 102, 17 475–17 487, 1997a.

Lockwood, M. and Carlson, Jr., H. C.: Production of polar cap electron density patches by transient magnetopause reconnection, Geophys. Res. Lett., 19, 1731–1734, 1992.

Lockwood, M. and Carlson, Jr., H. C.: Reply: ionospheric effects of transient magnetopause reconnection, Geophys. Res. Lett., 21, 2337–2338, 1994.

Lockwood, M. and Davis, C. J.: On the longitudinal extent of magnetopause reconnection bursts, Ann. Geophysicae, 14, 865–878, 1996.

Lockwood, M. and Hapgood, M. A.: How the Magnetopause Transition Parameter Works, Geophys. Res. Lett., 24, 373–376, 1997.

Lockwood, M. and Hapgood, M. A.: On the Cause of a Magnetospheric Flux Transfer Event, Geophys. Res., 103, 26 453–26 478, 1998.

Lockwood, M. and Opgenoorth, H. J.: Principles of combined ground-based and satellite studies of solar-terrestrial phenomena, ESA SP-1198 Ground-based observations in support of the Cluster mission, (Eds) Lockwood, M., Wild, M. N. and Opgenoorth, H. J., pp. 3–14, ESA Publications, ESTEC, Nordvijk, The Netherlands, 1997.

Lockwood, M. and Smith, M. F.: The variation of reconnection rate at the dayside magnetopause and cusp ion precipitation, J. Geophys. Res., 97, 14 841–14 847, 1992.

Lockwood, M. and Smith, M. F.: Low- and mid-altitude cusp particle signatures for general magnetopause reconnection rate variations: I – Theory, J. Geophys. Res., 99, 8531–8555, 1994.

Lockwood, M. and Wild, M. N.: On the quasi-periodic nature of magnetopause flux transfer events, J. Geophys. Res., 98, 5935–5940, 1993.

Lockwood, M., Sandholt, P. E., and Cowley, S. W. H.: Dayside auroral activity and momentum transfer from the solar wind, Geophys. Res. Lett., 16, 33–36, 1989a.

Lockwood, M., Sandholt, P. E., Cowley, S. W. H., and Oguti, T.: Interplanetary magnetic field control of dayside auroral activity and the transfer of momentum across the dayside magnetopause, Planet. Space Sci., 37, 1347–1365, 1989b.

Lockwood, M., Cowley, S. W. H., Sandholt, P. E., and Lepping, R. P.: The ionospheric signatures of flux transfer events and solar wind dynamic pressure changes, J. Geophys. Res., 95, 17 113–17 136, 1990.

Lockwood, M., Carlson, H. C., and Sandholt, P. E.: The implications of the altitude of transient 630 nm dayside auroral emissions, J. Geophys. Res., 98, 15 571–15 587, 1993a.

Lockwood, M., Denig, W. F., Farmer, A. D., Davda, V. N., Cowley, S. W. H., and Lühr, H.: Ionospheric signatures of pulsed magnetic reconnection at the Earth's magnetopause, Nature, 361 (6411), 424–428, 1993b.

Lockwood, M., Moen, J., Cowley, S. W. H., Farmer, A. D., Løvhaug, U. P., Lühr, H., and Davda, V. N.: Variability of dayside convection and motions of the cusp/cleft aurora, Geophys. Res. Lett., 20, 1011–1014, 1993c.

Lockwood, M., McCrea, I. W., Millward, G. H., Moffett, R. J., and Rishbeth, H.: EISCAT observations of ion composition and temperature anisotropy in the high-latitude F-region, J. Atmos. Terr. Phys., 55, 895–906, 1993d.

Lockwood, M., Cowley, S. W. H., Sandholt, P. E., and Løvhaug, U. P.: Causes of plasma flow bursts and dayside auroral transients: an evaluation of two models invoking reconnection pulses and changes in the Y-component of the magnetosheath field, J. Geo-

phys. Res., 100, 7613–7626, 1995a.

Lockwood, M., Cowley, S. W. H., Smith, M. F., Rijnbeek, R. P., and Elphic, R. C.: The contribution of flux transfer events to convection, Geophys. Res. Lett., 22, 1185–1188, 1995b.

Lockwood, M., Davis, C. J., Onsager, T. G., and Scudder, J. A.: Modelling signatures of pulsed magnetopause reconnection in cusp ion dispersion signatures seen at middle altitudes, Geophys. Res. Lett., 25, 591–594, 1998.

Lockwood, M., McCrea, I. W., Milan, S. E., Moen, J., Cerisier, J.-C., and Thorolfsson, A.: Plasma structure within poleward-moving cusp-cleft auroral transients: EISCAT Svalbard radar observations and an explanation in terms of large local time extent of events, Ann. Geophysicae, 18, 1027–1042, 2000.

Lockwood, M., Fazakerley, A., Opgenoorth, H., et al.: Coordinated Cluster and ground-based instrument observations of transient changes in the magnetopause boundary layer during an interval of predominantly northward IMF: relation to reconnection pulses and FTE signature, Ann. Geophysicae, this issue, 2001a.

Lockwood, M., Milan, S. E., Onsager, T., Perry, C. H., Scudder, J. A., Russell, C. T., and Brittnacher, M.: Cusp Ion Steps, Field-Aligned Currents And Poleward-Moving Auroral Forms, J. Geophys. Res., in press, 2001b.

McCrea I. W., Lester, M., Robinson, T. R., St.-Maurice, J.-P., Wade, N. M., and Jones, T. B.: Derivation of the ion temperature partition coefficient ßpara from the study of ion frictional heating events, J. Geophys. Res., 98, 15 701–15 715, 1993.

McCrea, I. W. and Lockwood, M.: Incoherent Scatter Radars, ESA SP-1198, Ground-based observations in support of the Cluster mission, (Eds) Lockwood, M., Wild, M. N., and Opgenoorth, H. J., ESA Publications, ESTEC, Nordvijk, The Netherlands, pp. 239–266, 1997.

McCrea, I. W., Lockwood, M., Moen, J., Pitout, F., Eglitis, P., Aylward, A. D., Cerisier, J.-C., Thorolfsson, A., and Milan, S. E.: ESR and EISCAT observations of the response of the cusp and cleft to IMF orientation changes, Ann. Geophysicae, 18, 1009–1026, 2000.

McEwen, D. J. and Harris, D. P.: Occurrence patterns of F-region patches over the north magnetic pole, Radio Sci., 31, 619–628, 1996.

McWilliams, K. A., Yeoman, T. K., and Provan, G.: A statistical survey of dayside pulsed ionospheric flows as seen by the CUTLASS Finland HF radar, Ann. Geophysicae, 18, 445–453, 2000.

McWilliams, K. A., Yeoman, T. K., and Cowley, S. W. H.: Two-dimensional electric field measurement in the ionospheric footprint of a flux transfer event, Ann. Geophysicae, 18, 1584–1598, 2001a.

McWilliams, K. A., Milan, S. E., Yeoman, T. K., Sigwarth, J. B., Frank, L. A., and Brittnacher, M.: IMF B_Y dependence of the relative position of the dayside ultraviolet auroral oval and the HF radar cusp, J. Geophys. Res., in press, 2001b.

Mende, S. B. et al.: Far ultraviolet imaging from the IMAGE spacecraft, Space Science Reviews, 91, 243–318, 2000.

Mersmann, U., Baumjohann, W., Küppers, F., and Lange, K.: Analysis of an Eastward Electrojet by Means of Upward continuation of ground-based magnetometer data, J. Geophys., 45, 281–298, 1976.

Milan S. E., Lester, M., Cowley, S. W. H., Moen, J., Sandholt, P. E., and Owen, C. J.: Meridian-scanning photometer, coherent HF radar, and magnetometer, observations of the cusp: a case study, Ann. Geophysicae, 17, 159–172, 1999.

Milan, S. E., Lester, M., Cowley, S. W. H., and Brittnacher, M.: Convection and auroral response to a southward turning of the

IMF, Polar UVI, CUTLASS and IMAGE signatures of flux transfer events, J. Geophys. Res., 105, 15 741–15 756, 2000.

Millward, G. H., Moffett, R. J., Balmforth, H. F., and Rodger, A. S.: Modelling the ionospheric effects of ion and electron precipitation in the cusp, J. Geophys. Res., 104, 24 603–24 612, 1999.

Moen, J., Sandholt, P. E., Lockwood, M., Denig, W. F., Løvhaug, U. P., Lybekk, B., Egeland, A., Opsvik, D., and Friis-Christensen, E.: Events of enhanced convection and related dayside auroral activity, J. Geophys. Res., 100, 23 917–23 934, 1995.

Moen, J., Lockwood, M., Sandholt, P. E., Løvhaug, U. P., Denig, W. F., van Eyken, A. P., and Egeland, A.: Variability of dayside high-latitude convection associated with a sequence of auroral transients, J. Atmos. Terr. Phys., 58, 85–96, 1996a.

Moen, J., Evans, D., Carlson, H. C., and Lockwood, M.: Dayside moving auroral transients related to LLBL dynamics, Geophys. Res. Lett., 23, 3247–3250, 1996b.

Morley, S. K. and Lockwood, M.: Concerning the effect of amplitude of reconnection rate pulses on cusp ion step signatures, Ann. Geophysicae, submitted, 2001.

Newell, P. T. and Meng, C. I.: Ion acceleration at the equatorward edge of the cusp: low altitude observations of patchy merging, Geophys. Res. Lett., 18, 1829–1832, 1991.

Newell, P. N. and Sibeck, D. G.: B_Y fluctuations in the magnetosheath and azimuthal flow velocity transients in the dayside ionosphere, Geophys. Res. Lett., 20, 1719–1723, 1993.

Ogawa, T., Buchert, S. C., Nishitani, N., Sato, N., and Lester, M.: Plasma density suppression process around the cusp revealed by simultaneous CUTLASS and EISCAT Svalbard radar observations, J. Geophys Res., 106, 5551–5564, 2001.

Onsager T. G., Kletzing, C. A., Austin, J. B., and MacKiernan, H.: Model of magnetosheath plasma in the magnetosphere: Cusp and mantle particles at low-altitudes, Geophys. Res. Lett., 20, 479–482, 1993.

Onsager, T. G. and Lockwood, M.: High-latitude particle precipitation and its relationship to magnetospheric source regions, Space Sci. Rev., 80, 77–107, 1997.

Onsager, T. G., Scudder, J. D., Lockwood, M., and Russell, C. T.: Reconnection at the High-Latitude Magnetopause During Northward IMF Conditions, J. Geophys. Res., submitted, 2001.

Opgenoorth, H. J., Lockwood, M., Alcaydé, D., et al.: Coordinated ground-based, low altitude satellite and Cluster observations on global and local scales, during a transient postnoon sector excursion of the magnetospheric cusp, Ann. Geophysicae, this issue, 2001.

Peredo, M., Slavin, J. A., Mazur, E., and Curtis, S. A.: Three-dimensional position and shape of the bow shock and their variation with Alfvénic and magnetosonic Mach numbers and interplanetary magnetic field orientation, J. Geophys. Res., 100, 7907, 1995.

Pinnock M., Rodger, A. S., Dudeney, J. R., Baker, K. B., Newell, P. T., Greenwald, R. A., and Greenspan, M. E.: Observations of an enhanced convection channel in the cusp ionosphere, J. Geophys. Res., 98, 3767–3776, 1993.

Pinnock, M., Rodger, A. S., Dudeney, J. R., Rich, F., and Baker, K. B.: High spatial and temporal resolution observations of the ionospheric cusp, Ann. Geophysicae, 13, 919–925, 1995.

Prikryl, P., MacDougall, J. W., Grant, I. F., Steele, D. P., Sofko, G. J., and Greenwald, R. A.: Observations of polar patches generated by solar wind Alfvén wave coupling to the dayside magnetosphere, Ann. Geophysicae, 17, 463–489, 1999a.

Prikryl, P., MacDougall, J. W., Grant, I. F., Steele, D. P., Sofko, G. J., and Greenwald, R. A.: Polar patches generated by solar wind Alfvén wave coupling to the dayside magnetosphere, Adv. Space Res., 23, 10, 1777–1780, 1999b.

Prikryl, P., Provan, G., McWilliams, K. A., and Yeoman, T. K.: Ionospheric cusp flows pulsed by solar wind Alfvén waves, Ann. Geophysicae, submitted, 2001.

Provan, G., Yeoman, T. K., and Milan, S. E.: CUTLASS Finland radar observations of the ionospheric signatures of flux transfer events and resulting plasma flows, Ann. Geophysicae, 16, 1411–1422, 1998.

Provan G., Yeoman, T. K., and Cowley, S. W. H.: The influence of the IMF B_Y component on the location of pulsed ionospheric flows in the dayside ionosphere observed by HF radars, Geophys. Res. Lett., 26, 521–524, 1999.

Provan, G. and Yeoman, T. K.: Statistical observations of the MLT, latitude and size of pulsed ionospheric flows with CUTLASS Finland radar, Ann. Geophysicae, 17, 855–867, 1999.

Rème, H., et al.: The Cluster Ion Spectrometry (CIS) Experiment by Space, Science Reviews, 79, 303–350, 1997.

Rème, H., Aoustin, C., Bosqued, I., et al.: First Multispacecraft Ion Measurements in and near the Earth's Magnetosphere with the Cluster Ion Spectrometry (CIS) Experiment, Ann. Geophysicae, this issue, 2001.

Rodger, A. S., Pinnock, M., Dudeney, J. T., Watermann, J., de la Beaujardiére, O., and Baker, K. B.: Simultaneous two hemisphere observations of the presence of polar patches in the nightside ionosphere, Ann. Geophysicae, 12, 642–648, 1994a.

Rodger, A. S., Pinnock, M., and Dudeney, J. T.: Comments on "Production of polar cap electron density patches by transient magnetopause reconnections", Geophys. Res. Lett., 21, 2335–2336, 1994b.

Rodger, A. S., Pinnock, M., Dudeney, J. T., Baker, K. B., and Greenwald, R. A.: A new mechanism for polar patch formation, J. Geophys. Res., 99, 6425, 1994c.

Ruohoniemi, J. M., Greenwald, R. A., Baker, K. B., Villain, J.-P., Hanuise, C., and Kelley, J. D.: Mapping high latitude plasma convection with coherent HF radars, J. Geophys. Res., 94, 13 463, 1989.

Sandholt, P. E., Lockwood, M., Denig, W. F., Elphic, R. C., and Leontjev, S.: Dynamical auroral structure in the vicinity of the polar cusp: multipoint observations during southward and northward IMF, Ann. Geophysicae, 10, 483–497, 1992.

Saunders, M. A.: The origin of cusp Birkeland currents, Geophys. Res. Lett., 16, 151–154, 1989.

Schunk, R. W., Raitt, W. J., and Banks, P. M.: Effect of electric fields on the daytime high latitude E- and F-regions, J. Geophys., Res., 80, 3121, 1975.

Shirai, H., Maezawa, K., Fujimoto, M., Mukai, T., Yamamoto, T., Saito, Y., and Kokubun, S.: Entry process of low-energy electrons into the magnetosphere along open field lines: polar rain electrons as field line tracers, J. Geophys. Res., 103, 4379–4390, 1998.

Shue, J.-H., Chao, J. K., Fu, H. C., Russell, C. T., Song, P., Kurana, K. K., and Singer, H. J.: A new functional form to study the solar wind control of the magnetopause size and shape, J. Geophys. Res., 102, 9497, 1997.

Sojka, J. J., Bowling, M. D., Schunk, R. W., Decker, D. T., Valladares, C. E., Sheehan, R., Anderson, D. N., and Heelis, R. A.: Modeling polar cap F-region patches using time varying convection, Geophys. Res. Lett. 20, 1783–1786, 1993.

Sojka, J. J., Bowline, M. D., and Schunk, R. W.: Patches in the polar ionosphere: UT and seasonal dependence, J. Geophys. Res., 99, 14 959–14 970, 1994.

Stauning, P.: Coupling of IMF B_Y variations into the polar iono-
spheres through interplanetary field-aligned currents, J. Geo-
phys. Res., 99, 17 309–17 322, 1994.

Stauning, P., Friis-Christensen, E., Rasmussen, O., and Venner-
strøm, S.: Progressing polar convection disturbances: Signature
of an open magnetosphere, J. Geophys. Res., 99, 11 303–11 317,
1994.

Stauning, P., Clauer, C. R., Rosenberg, T. J., Friis-Christensen, E.,
and Sitar, R.: Observations of solar-wind-driven progression of
interplanetary magnetic field B_Y-related dayside ionospheric dis-
turbances, J. Geophys. Res., 100, 7567–7585, 1995.

Syrjäasuo, M. T., Pulkkinen, T. I., Janhunen, P., Viljanen, A., Pelli-
nen, R. J., Kauristie, K., Opgenoorth, H. J., Wallman, S., Eglitis,
P., Karlsson, P., Amm, O., Nielsen, E., and Thomas, C.: Obser-
vations of substorm electrodynamics using the MIRACLE net-
work, in: Substorms-4, (Eds) Kokubun, S. and Kamide, Y., Terra
Scientific Publishing Company, Tokyo, pp. 111–114, 1998.

Valladares C. E., Basu, S., Buchau, S., and Friis-Christensen, E.:
Experimental evidence for the formation and entry of patches
into the polar cap, Radio Sci, 29, 167–194, 1994.

Watermann, J., de la Beaujardiére, O., and Newell, P. T.: Incoher-
ent scatter radar observations of ionospheric signatures of cusp-
like electron precipitation, J. Geomag. Geoelect., 44, 1195–1206,
1992.

Watermann, J., de la Beaujardiére, O., Lummerzheim, D., Woch,
J., Newell, P. T., Potemra, T. A., Rich, F. J., and Shapshak, M.:
The dynamic cusp at low altitudes: a case study utilizing Viking,
DMSP-D7, and Sondrestrom incoherent scatter radar observa-
tions, Ann. Geophysicae, 12, 1114–1157, 1994.

Weber, E. J. et al.: F-layer ionisation patches in the polar cap, J.
Geophys. Res., 89, 1683–1694, 1984.

Whitteker. J. H.: The transient response of the topside ionosphere
to precipitation, Planet. Space Sci., 25, 773–768, 1977.

Wickwar, V. B. and Kofman, W.: Dayside auroras at very high lati-
tudes: the importance of thermal excitation, Geophys. Res. Lett.,
11, 923–926, 1984.

Wing, S., Newell, P. T., and Onsager, T. G.: Modelling the entry
of the magnetosheath electrons into the dayside ionosphere, J.
Geophys. Res., 101, 13 155–13 168, 1996.

Yeoman, T. K., Lester, M., Cowley, S. W. H., Milan, S. E., Moen,
J., and Sandholt, P. E.: Simultaneous observations of the cusp
in optical, DMSP and HF radar data, Geophys. Res. Lett., 24,
2251–2254, 1997.